NASA CR-86334

FEASIBILITY MODEL OF AN ADVANCED CROSSED-FIELD AMPLIFIER FOR SPACE COMMUNICATION SYSTEMS

by
G. Bernstein
H. McDowell
T. Schultz

January 1970

Prepared under Contract No. NAS12-653
by
S-F-D laboratories/A Varian Division
800 Rahway Avenue
Union, New Jersey

Electronics Research Center
Cambridge, Massachusetts

National Aeronautics and Space Administration

Technical Monitor, NAS12-653

C.M. Veronda, Chief
Circuits and Antennas Branch
Optics and Microwave Laboratory
Electronics Research Center
575 Technology Square
Cambridge, Massachusetts 02139

Requests for copies of this report should be referred to

NASA Scientific and Technical Information
Facility
P.O. Box 33
College Park, Maryland 20740

NASA CR-86334

FEASIBILITY MODEL OF AN ADVANCED CROSSED-FIELD AMPLIFIER FOR SPACE COMMUNICATION SYSTEMS

by

G. Bernstein
H. McDowell
T. Schultz

January 1970

Prepared under Contract No. NAS12-653
by
S-F-D laboratories/A Varian Division
800 Rahway Avenue
Union, New Jersey

Electronics Research Center
Cambridge, Massachusetts

National Aeronautics and Space Administration

ABSTRACT

This report presents the results of a program to develop and demonstrate a feasibility model of a new form of crossed-field amplifier suitable for use in AM or RM transmitters.

The use of an external beam injection scheme combined with a multi-element collector structure provides the mechanism for achieving a high conversion efficiency over a wide dynamic range of RF drive levels.

The evolution of the design, the experimental results and recommendations for further development of this type of amplifier are included in the report.

During the program, a power output of over 2 kw with a saturated power gain over 20 db was obtained. The maximum efficiency observed was over 70%, although noise power generation at this operating mode did not allow simultaneous demonstration of wide dynamic range and zero signal stability. Wide dynamic range and zero signal stability were demonstrated with reduced efficiency. Methods to obtain all desirable characteristics simultaneously are suggested and preliminary investigations of these methods were conducted. The basic feasibility of the axial injected beam crossed-field amplifier has been demonstrated and satisfactory performance obtained for a saturated amplifier. Further work is required to obtain dynamic range.

TABLE OF CONTENTS

LIST OF ILLUSTRATIONS

1.0 INTRODUCTION

This is the final report on a program to develop and demonstrate a feasibility model of an advanced crossed-field amplifier capable of high conversion efficiency and wide dynamic range. The amplifier was to be suitable for use in TV communication transmitters using either AM or FM as the modulation mode. This program was carried out for the NASA (Cambridge) Electronic Research Center under Contract NAS12-653.

1.1 Program Objectives

The following were the primary objectives to be demonstrated by the experimental crossed-field amplifier.

1.1.1 Frequency

The amplifier design to be evolved was to be compatible with operation either in the UHF range (0.5 GHz to 1.5 GHz) or at S-band (2.5 GHz to 3.2 GHz). The contract stipulated that in order to achieve a minimum program cost, a demonstration at an alternate frequency could be chosen if the design were such that it could be readily scaled to the above frequency ranges. The actual experimental amplifier was built to operate at the lower end of the UHF range, 300 MHz.

1.1.2 Power Output

The power objectives of the program included a peak power output of 5 kw corresponding to the synchronizing pulse level, and an average power capability of 1.6 kw to fit an assumed average TV signal.

1.1.3 RF Bandwidth

The instantaneous 1 db bandwidth was to be 40 MHz with the indication that 180 MHz would be desirable with anode voltage adjustment.

1.1.4 Conversion Efficiency

An efficiency of at least 65% at peak synchronizing saturation level was sought, with greater than 50% to be obtained at the assumed average TV level of one-third of this saturation level. The conversion efficiency is defined as the RF power output minus the RF power input divided by the total prime power input.

1.1.5 Power Gain

A minimum of 14 db of gain was established.

1.1.6 Dynamic Range

The dynamic range was to be 20 db for an AM signal.

1.1.7 Stability

Zero signal stability was to be exhibited with an output VSWR of 2:1.

1.1.8 Linearity

Linearity was to be such that standard communication noise loading power ratio or two tone tests would exhibit results in excess of 40 db.

1.1.9 Modulation Capability

The tube was to have capabilities adequate to handle amplitude modulation requiring a 6 MHz bandwidth or FM modulation requiring a 40 MHz bandwidth.

1.1.10 Weight, Size, Cooling, and Environment

The factors of weight, size, cooling, and compatibility with space environment were to be considered in the basic design but were not primary considerations in this demonstration amplifier.

1.1.11 Life

A design consistent with a minimum of two years of continuous operation was part of the goal of this program. However, it was not required of the feasibility model.

1.2 Approach Chosen to Meet Program Objective

The amplifier chosen as being best suited to meet all of the objectives of the program was the axial injection crossed-field amplifier. This specific format of crossed-field amplifier (CFA) was developed by S-F-D laboratories. Early background experience for the choice of this tube type was established by low power experiments sponsored by S-F-D laboratories. In addition, an initial theoretical investigation on the use of the axial injection CFA in a TV satellite transmitter was carried out for the NASA Lewis Research Center under Contract NAS3-11516.

The axial injection crossed-field amplifier generates the electron stream in the interaction space not by thermionic or secondary emission from the sole element, but by injection of a hollow beam generated in a magnetron injection gun. The beam is injected into the interaction space parallel to the magnetic field and the axis of symmetry of the circular tube. This means of injection is highly similar to that used in the voltage tunable magnetron. In the original concept, the current was to be collected after making one axial transit through the interaction space. It appeared that this approach would yield the desired operating characteristics. Some of these characteristics were available in various other types of crossed-field amplifiers but not all of them in one type.

The design approach taken makes it possible to achieve the very high saturation conversion efficiency and compact size of the emitting sole crossed-field amplifier. However emitting sole CFAs are not zero signal stable and have no dynamic range.

The control of beam current and space charge density made possible by the external magnetron injection gun provides the means to obtain zero signal stability and an extended linear dynamic range.

The life capabilities of the axial injection electron gun are similar to the demonstrated long life capabilities of thermionic cathodes as used in linear beam microwave tubes, such as klystrons and traveling wave tubes.

The use of an appropriately designed multi-element collector makes possible the control of dc power input as a function of the RF drive level, thus maintaining a high level of efficiency at drive levels below the saturation value. This is of particular importance in the case of an amplitude modulated TV signal where the average power level is 5 db below the peak synchronizing pulse.

The required RF bandwidth was obtained by the choice of an appropriate forward wave delay line, for use as the anode of the tube. Crossed-field amplifiers of many varieties have demonstrated instantaneous bandwidths far in excess of that required by this program.

The concept of injecting the current continuously along the length of the RF circuit makes possible a reduced value of emission density which greatly enhances the ability of the tube to meet the extensive life requirements of the amplifier. A more extended discussion of the various features of the axial injection crossed-field amplifier will be given in Section 2 of this report.

The initial design activities on this program included the selection of a helix loaded bar circuit of existing design as the slow wave circuit to be used in the amplifier. The design of the optics of the magnetron injection gun and the six-element collector system were also carried out. The detailed results of the electron gun analysis, with respect to axial velocity distribution in the beam, eventually led to modification of some of the original design concepts concerning removal of the beam after one axial passage. The beam

trajectory calculations were implemented with a digital computer program which is in use for doing electron trajectory tracing in an axial injection geometry. The calculation of the small signal interaction parameters and large signal performance was carried out for various conditions of axial velocity spread within the beam. The large signal calculations were carried out with a digital computer program which has capabilities for handling both the space charge and no space charge cases. Some of the later analytical design activities were supplemented by a study program sponsored by the NASA Lewis Research Center under Contract NAS3-11528, particularly in the area of some of the digital computer simulations.

The experimental test vehicle incorporating the six-element collector was built and tested. A discussion and evaluation of the test results are given in Section 3 of this report.

2.0 DESIGN OF THE EXPERIMENTAL AMPLIFIER

The design phase of this program was concerned with the following major areas:

Select suitable forward wave delay line that would have high interaction impedance, low insertion loss, and thermal properties compatible with a space environment waste heat disposal system.

Design the magnetron injection gun and analyze the resulting beam trajectories and velocity distributions within the gun.

Select tube operating parameters and calculate expected small signal performance, small signal gain, and diocotron gain level.

Calculate large signal response and estimate conversion efficiencies.

Design suitable multi-element collector system for experimental flexibility.

Arrive at a mechanical design which would allow reuse of the test vehicle.

Before examining each of these design areas in detail, a short review of axial injection CFA concepts follows.

2.1 Operating Principles of the Axial Injection CFA

Figure 1 shows a schematic drawing of an axial injection amplifier as originally proposed for this program. Beam trajectories shown are those obtained with a low RF input signal. The tube is constructed in circular format with a slow wave circuit or delay line forming most of the circumference of the anode. The delay line is at ground potential. Located concentrically within the delay line is a non-emitting sole element. The sole is operated at a potential negative with respect to the delay line so that a radial dc electric field exists between the sole and the delay line. In conjunction with an axial magnetic field, this provides the crossed-field interaction

characteristics of a CFA. An electron gun employing a thermionic cathode is mounted concentric with the interaction space, but axially is displaced to one end of it. A concentric multi-section collector is located at the opposite end.

Figure 2 shows a cross section through the interaction space at the plane A-A of Figure 1. In this figure, the interaction space is shown as reentrant, allowing electrons to circulate from the output back to the input. Between the output and input there is a drift space whose purpose is to debunch the electron stream so that RF feedback from output to input is avoided. This structure is in contrast to the emitting sole crossed-field amplifier where the electron stream is generated by emission from the sole surface. In the structure sketched here, the surface is made non-emitting and is biased negative with respect to the cathode electrode. This prevents electrons from striking the sole which insures that it will be non-emitting. Operation with a biased sole means that the beam is some distance away from the sole surface. Since the sole surface acts as a shorting plane for the RF fields emanating from the delay line, a higher interaction impedance at the beam position is achieved.

As indicated in Figure 1, electrons from the gun are injected into the interaction space by a component of velocity, parallel to the tube axis, which is imparted to it by the electric fields of the magnetron injection gun. At the end of the interaction space opposite to the gun, there is indicated a collector assembly consisting of a number of rings. This is a multi-element collector in which the rings are meant to be operated at successively higher potentials ranging from cathode potential to anode potential. Electrons leaving the interaction space are collected on a ring at a potential close to that at which they leave the interaction space. In this manner, the energy dissipated on the collector segment is minimized. The dc power input for the various current elements is the amplitude of the current

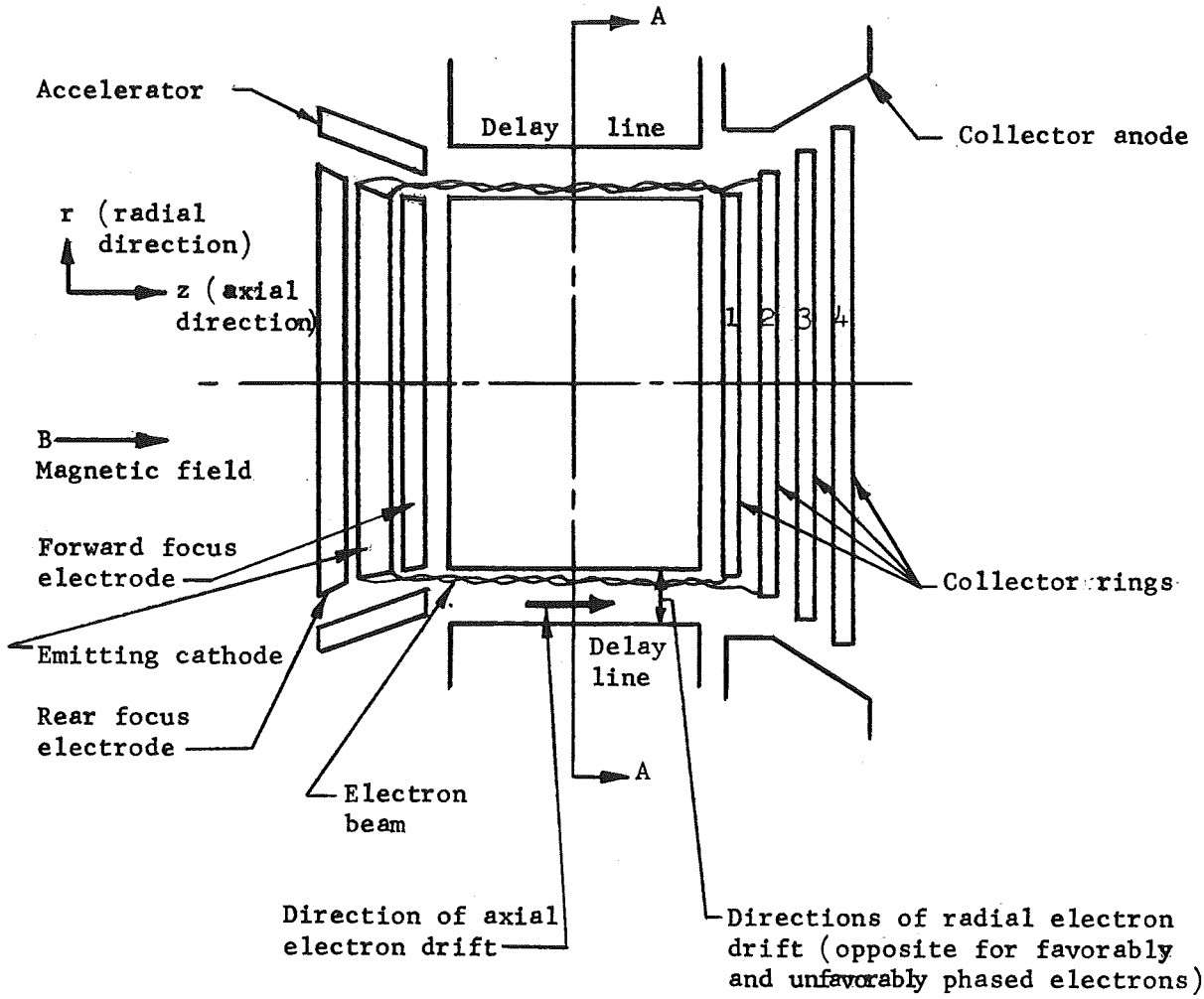

FIGURE 1 SKETCH OF AN AXIAL INJECTION CFA

Electron beam in interaction space circulates in the circumferential direction (perpendicular to paper) with a velocity greater than the axial (z direction) drift velocity. Trajectories are shown for a condition of low RF input drive

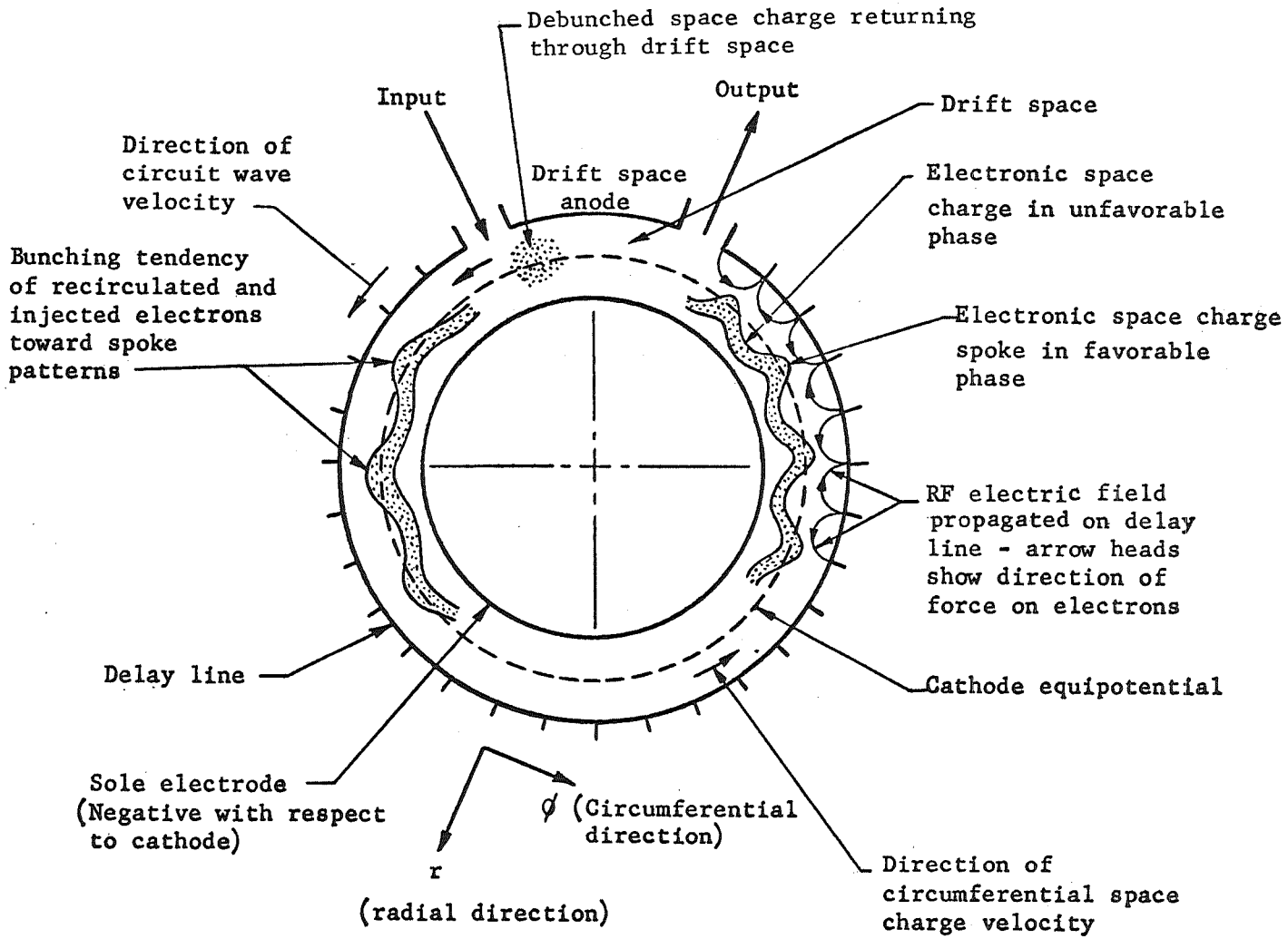

FIGURE 2 CROSS-SECTION THROUGH A-A IN FIGURE 1 SHOWING A SKETCH OF THE SPACE CHARGE DISTRIBUTION

multiplied by the voltage of the collecting element with respect to cathode potential. Since the radial position of the electron stream is a function of the RF drive level, it is thus seen that a mechanism for controlling the dc power input as a function of drive level is achieved. This makes possible a high level of conversion efficiency over a wide dynamic range and not merely at the saturation value of drive power. RF modulation of the electron stream in a crossed-field device results primarily in position modulation rather than velocity modulation of the stream, which results in the spent beam being readily amenable to multi-element collection schemes.

Electrons originating in the gun follow trajectories of the sort shown in the developed view, Figure 3. This sketch shows an interaction space which has been unwrapped and in which the viewer looks down upon the beam from the delay line to the sole. An electron acquires a circumferential drfit velocity equal to the ratio of electric to magnetic fields in the interaction space. The voltage and magnetic fields are adjusted so that this circumferential drift velocity is in synchronism with the velocity of the circuit wave, thus providing for the implementation of the usual crossed-field gain mechanism. The electron also has an axial drift velocity as a result of the electric fields in the gun and the fields which exist in the transition region between the gun and the interaction space. The operating parameters of the gun have an effect both on the amount of current injected and the axial drift velocity which is injected. The sketch of Figure 3 indicates that the circumferential drift velocity is several times greater than the axial drift velocity so that the electron travels through a significant fraction of the circumference of the tube before it is removed from the interaction space. If this ratio of circumferential to axial drift velocity is achievable, then an adequate component of circumferential circulating current can be established by one axial transit of the beam through the tube. If

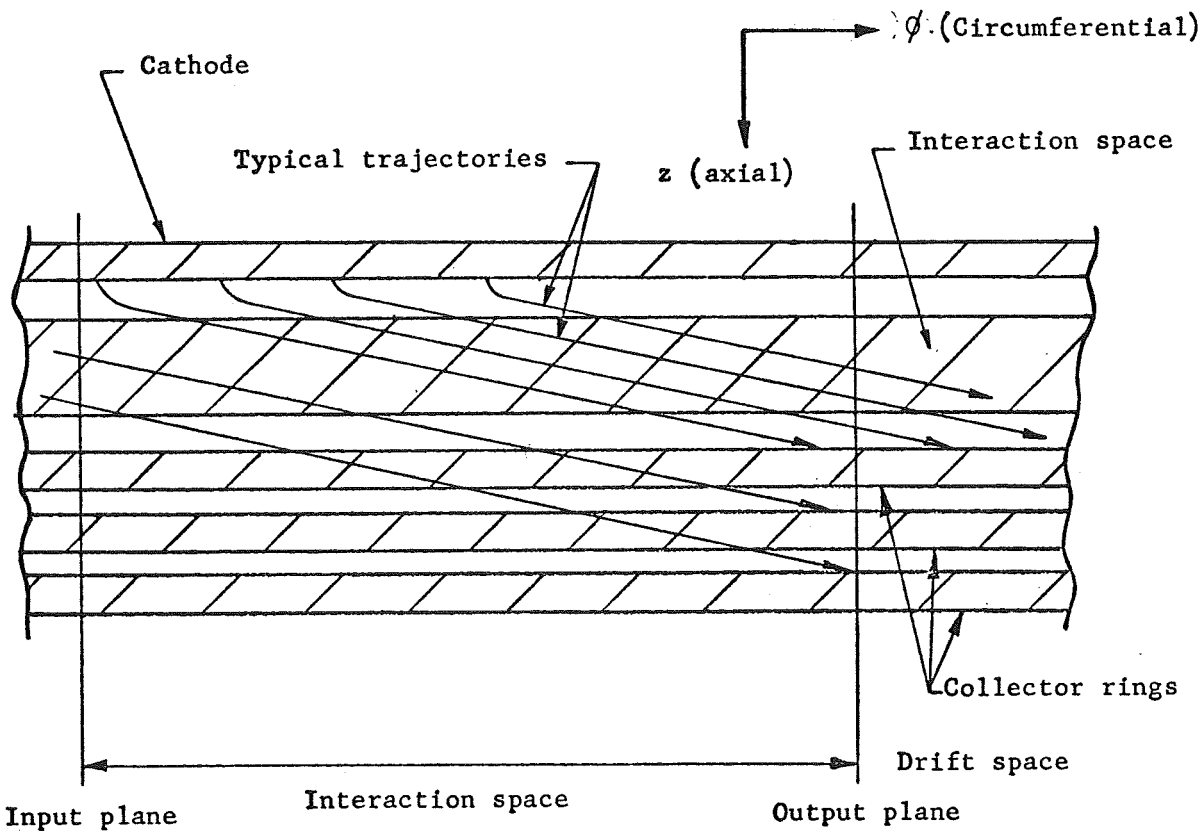

FIGURE 3 SKETCH OF THE INTERACTION SPACE WHICH HAS BEEN DEVELOPED (UNWRAPPED) IN THE ϕ-z PLANE.

We are looking from the delay line toward the sole.

this ratio of velocities is not possible, then the concept should be modified as discussed later in this report.

The axial drift velocity serves the purpose of transporting the electrons across the interaction space, from gun to collector region. This axial transport of electrons provides a means for achieving a controlled drainage of the electrons from the interaction space. This provides the means for achieving the necessary operating power level without allowing the space charge density in the interaction region to build up to the point where excessive noise levels can occur. This is the basic principle which will allow a large dynamic range, low noise level, and zero signal stability to be achieved.

The conversion of dc energy to RF energy occurs when there is a radial excursion of the electron stream from the sole toward the anode, thus giving up dc potential energy. This motion occurs under the influence of the RF fields. At low RF drive levels, this radial excursion is modest as indicated in Figures 1 and 2. The electron stream is collected by low potential collector elements, limiting the dc input under conditions of low RF drive.

The dynamics of the interaction process between the RF fields and the electron stream under conditions of large RF drive are as sketched in Figures 4 and 5. Those electrons which are traveling in the proper RF phase with the circuit wave move toward the delay line and are collected either upon the delay line or a high potential collector element. The unfavorably phased electrons acquire energy from the RF field, stay close to the sole and are, in turn, collected on a low potential collector element. Thus, only the electrons that are instrumental in generating large amounts of RF power draw the maximum amount of dc power from the power supply. An appropriate multi-tap power supply is used to supply the potentials to the collector elements.

These key elements of the axial injection crossed-field amplifier result in operating characteristics which are particularly

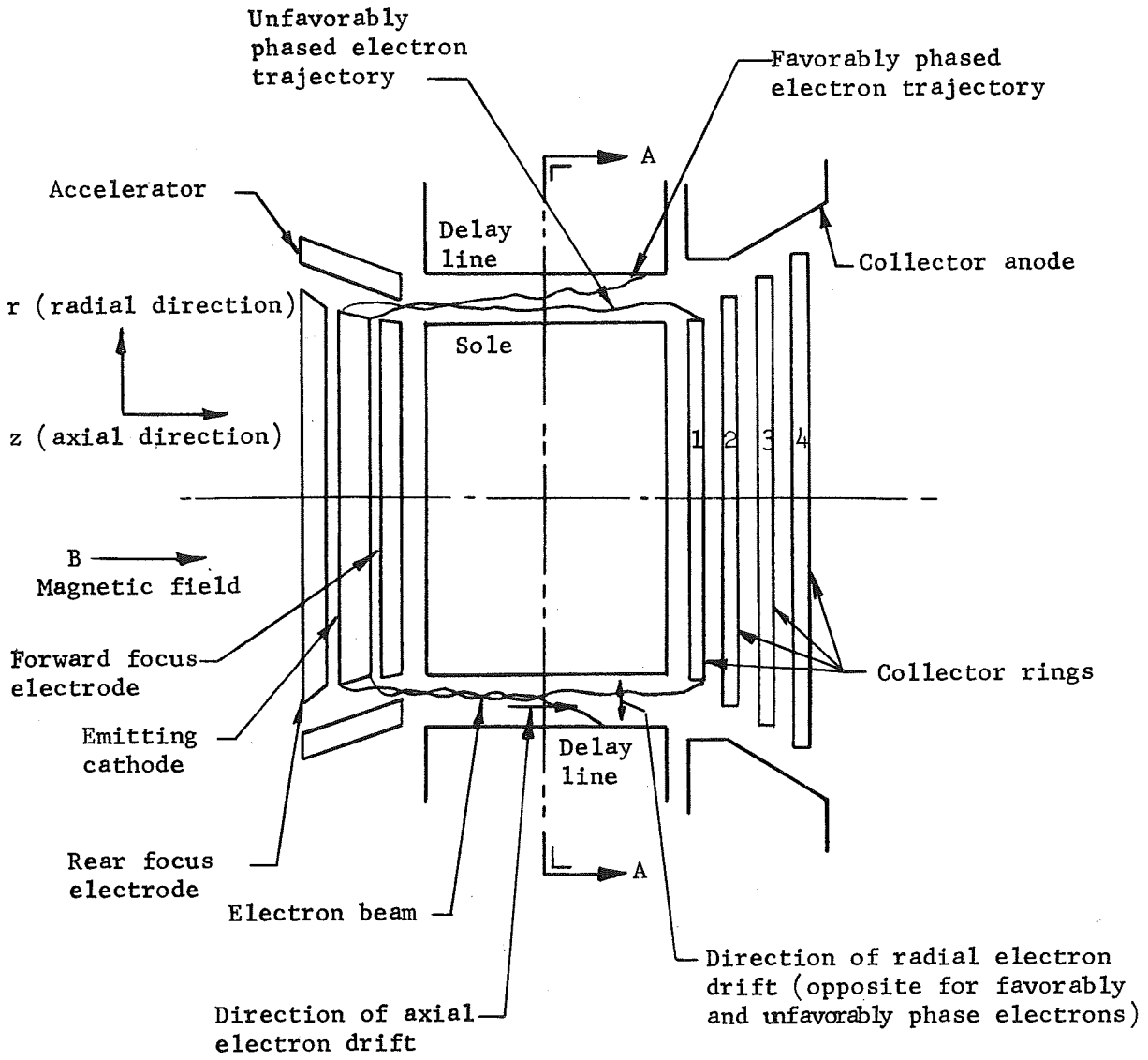

FIGURE 4 ELECTRON TRAJECTORIES WHEN THE TUBE IS DRIVEN TO SATURATION

The favorably phased electrons are collected on the delay line while the unfavorably phased electrons are collected on the first collector ring at cathode potential

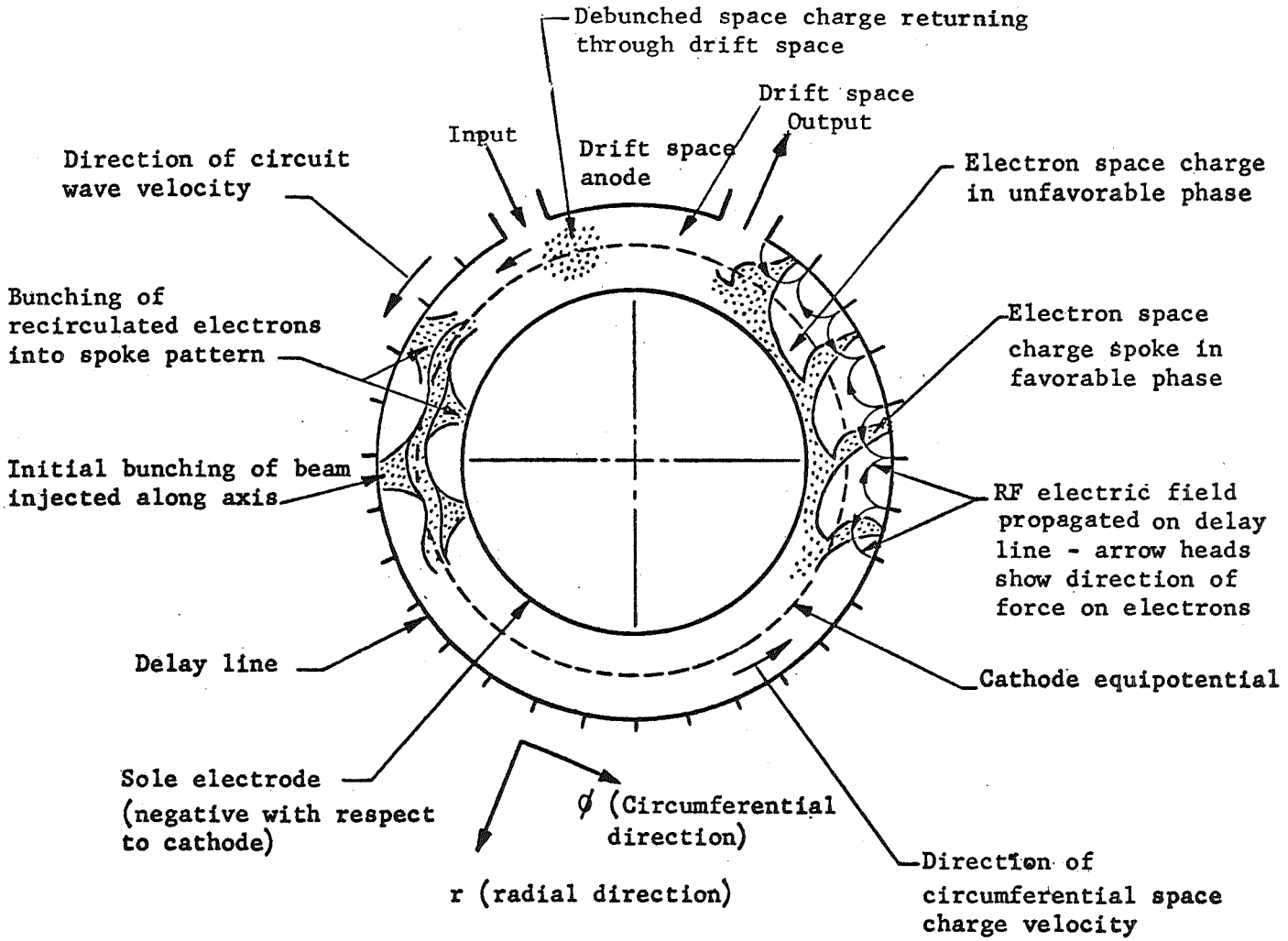

FIGURE 5 CROSS-SECTION THROUGH A-A IN FIGURE 4 SHOWING A SKETCH OF THE SPACE CHARGE DISTRIBUTION WHEN THE TUBE IS DRIVEN TO SATURATION

suitable for meeting the objectives of this program. The use of an electron beam injection scheme, coupled with controlled collection by a multi-element collecting system, can result in the control of background noise and the attainment of zero signal stability. The injected beam approach allows the voltage and current levels to be chosen independently. This is not always possible with the emitting sole type of amplifier.

Incorporation of a multiple electrode collector results in the maximizing of efficiency at every output power level rather than at just the saturation output level.

A high average power capability and long life assurance are realized through the minimizing of cathode current density and circuit dissipation because of the distributed emission injection scheme.

The removal of the electron source from the RF interaction space greatly enhances the assurance of long life operation. It is expected that an operating life comparable to that achieved by cathodes in O-type microwave tubes will be achieved.

During the course of this development, it became apparent that the concept of allowing the beam to undergo only one axial transit through the tube had best be modified in order to achieve optimum operation. This results from the fact that certain fundamental considerations place a lower limit on the average axial velocity of the electron beam and thus the average electron traverses only a fraction of the delay line length before emerging from the interaction space. The reasons for this limitation are discussed in Section 2.4. The effect of this limited circulation before exiting is indicated by some of the large signal calculations. A system which uses several axial reflections of the electron beam before collection will therefore be proposed as a design modification. This too is discussed in further detail in Section 3.0.

2.2 Selection of the Slow Wave Circuit

In order to achieve the objectives of this program at a minimum cost in circuit development and to make use of available test equipment, it was agreed to directly use one of the slow wave circuits that had been developed at S-F-D laboratories for operation in the UHF frequency region. This brought under consideration two possible delay lines, a helix of rectangular cross section and the helix loaded bar circuit. The helix loaded bar circuit was chosen as being best suited for this application. This circuit had maximum interaction impedance, minimum insertion loss necessary for high efficiency operation, and a thermal capability compatible with a space environment heat disposal system. Such a heat disposal system might consist of an array of heat pipes connected to the tube structure which lead the heat to an external radiating surface.

The superior thermal capability of the helix loaded bar circuit made it a design choice over the helix although the interaction impedance and insertion loss capabilities turned out to be similar. This choice is also consistent with the design conclusions arrived at on an earlier study program carried out for the NASA Lewis Research Center under Contract NAS3-11516.

The geometry of the helix coupled bar circuit is shown in Figure 6. The circuit consists of a series of thin capacitive metal bars mounted above a ground plane on slabs of ceramic. The ceramic used is beryllium oxide and provides a direct heat flow path to the metallic plate which acts both as a heat sink and the ground element in the artificial transmission line. The bars are connected to an inductive loading coil; thus the circuit is a quasi-lumped element transmission line. The equivalent circuit of this structure is shown at the top of Figure 6. As is indicated, the beam flows between the sole element of the crossed-field amplifier and the capacitive bars. The electron stream interacts with the RF field which fringes between

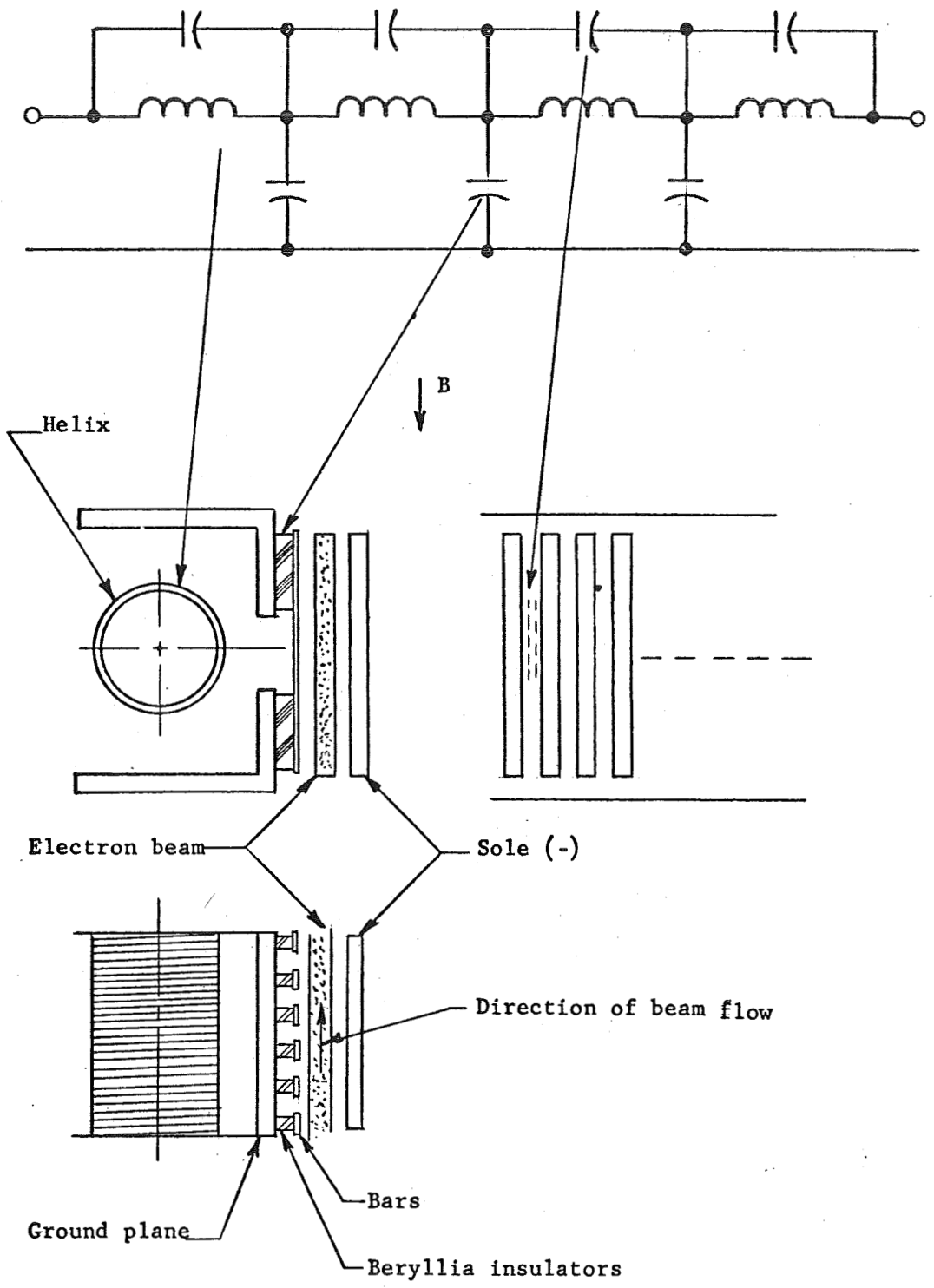

FIGURE 6 THE HELIX COUPLED BAR CIRCUIT

Sketch at the top shows the low frequency equivalent circuit of this line

the bar elements. These fields result from the voltage that exists across the series capacitance which is shown in the equivalent circuit. By an appropriate choice of capacitance, inductance per section of circuit, and mutual inductance between sections of circuit, the impedance characteristics and insertion loss of the bar circuit may be made highly similar to that of the helix. An additional factor which favored the use of the loaded bar circuit in this program was that the impedance transformers between the high surge impedance of the delay line and the 50 ohm external system were mounted outside the vacuum envelope of the tube. This meant that experimental flexibility was available so that external adjustments of the match could be achieved after the tube had been processed.

Thus, the design was fixed for an operating frequency of 300 MHz with the bar circuit having the following operating parameters.

Interaction impedance at 300 MHz	130 ohms
Synchronous voltage of delay line	290 v
Approximate insertion loss of delay line	1.5 db
Circuit pitch	0.324"
Circuit height	2.1"
Number of active sections	69
Active circuit length	22.4"
Loading coil	Two turns per section

Since the delay line chosen for the experimental demonstration was selected from available structures at S-F-D laboratories, the synchronous voltage of the available circuit was somewhat lower than the design value that might normally have been chosen for the 5 kw of peak power output. That is, the current that would be necessary to generate 5 kw of peak power output with the 290 v circuit was sufficiently high that the possibility of developing some background noise arose. Therefore, it was agreed to proceed with the demonstration amplifier

limiting the experimental evaluation of the device to an operating level of 2 kw of peak power. The design of the electron gun and other elements of the amplifier was made consistent with the 2 kw power level. For the 5 kw power level, the optimum design would be scaled to a somewhat higher voltage, thus reducing the required current and providing a lower diocotron gain level. The diocotron gain in the electron stream is the mechanism by which thermal noise is amplified in the electron stream of a crossed-field device.

2.3 Calculation of Operating Parameters and Tube Performance

A design objective of 20 db of gain for the amplifier was chosen. One reason for choosing this gain level as an operating parameter was that with the achievement of high conversion efficiency for the amplifier being developed, a high level of gain would make the system efficiency relatively insensitive to the efficiency of the device driving the amplifier. For example, if for a given operating power level, the efficiency of the amplifier is 75% and the efficiency of the driver tube is 25% at an output amplifier gain level of 20 db, then the net efficiency for the two-amplifier chain would be 72.8%. Another practical reason for choosing the 20 db of gain as a design objective was the existence of appropriate driver and test equipment at S-F-D laboratories corresponding to this level of gain. That this was a reasonable design objective will be seen from the discussion of the performance calculations that follow.

2.3.1 Small Signal Design Parameters

The approach used to calculate those aspects of the design which can be derived from small signal amplifier theory follows.

In the reentrant structure which allows the beam to exit from the interaction space after one axial transit, the ratio of effective circulating current in the interaction space to cathode current is

given by the number of revolutions which the electron makes along the circuit during the time for one axial transit. This relationship is illustrated more fully in Section 2.4. This ratio is used to estimate the effect of circulating current for a given value of cathode current in the small signal gain calculations.

Relationships used for calculating the small signal gain characteristics of the tube are summarized as follows.

$$\frac{\omega_c}{\omega} = \left[\frac{\frac{V_a}{V_o} - 1}{2\beta y_-} \right] \qquad (1)$$

where ω_c = cyclotron radian frequency = $(e/m)B$

B = operating magnetic field

e/m = charge-to-mass ratio for electron

V_a = cathode-anode voltage

V_o = synchronous voltage

$\beta = \omega/v_p$ = propagation constant of delay line

y_- = distance from top surface of beam to anode

$$D = \left[\frac{1}{2} \frac{\omega}{\omega_c} \frac{I_c}{V_o} K \right]^{\frac{1}{2}} e^{-\beta y_-} \qquad (2)$$

where D = gain parameter

I_c = circulating beam current

K = interaction impedance of circuit = $E^2/2\beta^2 P$

$$G = -6 - \frac{\alpha N}{2} + 55DN \text{ (db)} \qquad (3)$$

where G = small signal gain in db

α = insertion loss in db per circuit wavelength

N = number of wavelengths on circuit

$$I_c = (1.56)hBV_o(2)k\left(1 - \frac{k}{2}\right) \qquad (4)$$

where h = axial height of circuit

B = axial magnetic field

$k = \Delta v/v = 1 - \sqrt{1 - Q}$

v = circumferential velocity of outer surface of beam

Δv = difference in circumferential velocity between outer and inner surface of the beam

$Q = I_c/(1.56)hBV_o$

$$S = \frac{1}{2D}\frac{\Delta v}{v} \qquad (5)$$

where S = diocotron gain parameter

These relationships have been summarized in a time share computer program. In order to achieve a high level of conversion efficiency, a large ratio of operating cathode-anode voltage to synchronous voltage was chosen; i.e., 20 to 1. In the initial design considerations, the first round of calculations were carried out presuming that the electron stream would move 70% of the way around the circumference of the anode before exiting axially from the tube. When a more detailed analysis of the velocity distribution achievable in the beam was made, it appeared that on the average only about 8" of circuit length would be covered by a typical electron before exiting from the interaction space. This is an average value with some electrons covering more circuit length and some covering less. Thus, although the beginning design postulated a cathode current of about 1 ampere, this value was changed to a cathode current of 1.8 amperes in order to maintain a reasonable value of the circulating current, I_c. A summary of the listing of output values from the small signal program is given in Table I. Table II summarizes the small signal operating parameters using the results of the calculation.

TABLE I

PRELIMINARY DESIGN PROGRAM FOR INJECTED BEAM CFA

Delay line pitch = 0.324 in Delay line width = 2.100 in

Delay Line Characteristics as a Function of Frequency

Freq	Theta	Theta	K	Att/in	Sync Velocity	v/c	c/v	Sync Voltage
GHz	deg	rad	ohms	db/in	m/sec			volts
0.25	75.5	1.32	155.0	0.06	0.98×10^8	0.033	30.6	273.6
0.30	88.0	1.54	130.0	0.07	0.10×10^8	0.034	29.7	290.0
0.35	102.9	1.80	11.0	0.09	0.10×10^8	0.034	29.8	288.6

FRACLN = 8 in I_c/I_k = 0.32 I_c = 0.575 amp

Sole to anode spacing = 0.400 in
Line length = 22.40 in
Distance from line to top of beam = 0.240 in
Beam current = 0.575 amp
Current build up distance = 0.0 in
Total extra attenuation added to line = 0.0 db
Synchronous cathode voltage = 5.8 kv
Frequency 0.30 GHz chosen for synchronism
Magnetic field = 895 gauss
Cyclotron frequency = 2.51 GHz
Maximum permissible current = 2.156 amps
Ratio of current to max current = 0.27
Beam thickness = 0.0036 in
Sole voltage = 8662 v

Output Power at Various Efficiencies at Saturation

Efficiency - %	25	33	40	50
Power - w	834	1101	1334	1667

Characteristics as a Function of Frequency

Freq	FNorm	D	S	N	Sinh Fctn	Gain	DLBA
GHz						db	
0.250	0.100	0.04808	1.494	14.499	0.377	31.532	1.545
0.200	0.120	0.03975	1.807	16.900	0.320	30.029	1.325

TABLE II

SMALL SIGNAL OPERATING PARAMETERS

Circuit pitch	0.324 in
Circuit axial height	2.1 in
Phase shift per section at 300 MHz	88 deg
Circuit synchronous voltage at 300 MHz	290 v
Sole to anode spacing	0.4 in
Active line length	22.4 in
Distance from line to top of beam	0.24 in
Circumferential travel during one axial transit	8 in
Cathode current	1.8 amps
Circulating current	0.575 amps
Cathode-anode voltage	5.8 kv
Magnetic field	895 gauss
Percentage slip in circumferential velocity between the outer edge and inner edge of beam	0.14
Radial beam thickness	0.004 in
Sole anode voltage	8660 v
Small signal gain parameter, D at 300 MHz	0.04
Number of RF wavelengths at 300 MHz	16.9
S factor at 300 MHz	1.81
Gain at 300 MHz	30 db

Thus it is seen that this choice of parameters leads to a more-than-adequate initial prediction of small signal gain, a reasonable value of magnetic field with the electron beam placed a little more than half the distance from the sole to the anode, and a bias voltage of 2.8 kv between sole and cathode to assure that no back bombardment of the sole will occur from the electron stream.

The S parameter listed in the above tabulation is useful in predicting the noise-free qualities of the amplifier. Background noise in a crossed-field amplifier usually arises from the diocotron or slipping stream gain mechanism within the electron beam. It is this mechanism that may, under certain given conditions, amplify the background thermal noise to levels comparable to the RF signal being handled by the amplifier. An approximate model of the diocotron gain mechanism in a crossed-field amplifier is provided by Gould's analysis (Ref. 1). From this model, it may be deduced that the diocotron gain to be expected in a given beam and circuit configuration is given approximately by the S parameter multiplied by the expected amplifier gain of the device. The S parameter has already been defined as being equal to one half the relative velocity slip in the beam divided by the small signal gain parameter. Thus, with an S parameter of about 2 and a calculated small signal gain approaching 30 db, the estimated diocotron gain level would be on the order of 60 db. Thermal noise energy in a 6 MHz or even 40 MHz band amplified up by 60 db is still well below the specification set forth for the amplifier to be developed on this program.

A calculation of efficiency and gain using a large signal computer program was then undertaken.

2.3.2 Large Signal Calculations

The large signal computer program used at S-F-D laboratories to calculate the performance of a given axial injection system uses a Lagrangian approach. That is, the current is simulated by an array of

charge rods that enter the interaction space to simulate the electron beam. The program permits the rods to be arranged either in a single layer or in multiple layers and to simulate finite beam thickness and circumferential velocity slip within the beam. The radial position of this multi-layer beam is one of the input specifications. At the point along the circuit where current is to be injected, rods are introduced over 2π radians of phase angle corresponding to a single RF wavelength. This simulates entrance of the beam at all values of RF phase. Other input parameters to the program are the sole-anode and cathode-anode voltages and the magnetic field. The values of circuit interaction impedance and RF drive level are specified along with the pitch and phase shift per section of the circuit.

An iterative series of calculations then traces the cluster of electrons, within the frame of a single RF wavelength, down the delay line over the specified length of circuit. The circuit insertion loss is specified and taken into account and even circuit severs may be specified. The time step over which this calculation is iterated is also an input specification. The calculation may be carried out either with space charge forces ignored or taken into account.

The program simulates the velocity in the third or axial dimension and the process of distributed injection as follows. The rods are introduced in pairs at regular intervals along the circuit. Two rods which are injected at a given point on the transmission lines are placed π radians apart and are of opposite phase. Thus their introduction represents no RF information at the frequency of calculation. In addition a control variable is set up so that the amount of time that each pair of rods spends in the system is specified. Thus any charge rod that has been in the system a length of time equal to the time of axial transit through the tube is removed from the system and noted as having been collected by the collector structure or anode if it is collected on the anode before this time is up. The

program records the point at which this occurs, the wavelengths down the circuit, the radial and phase coordinates, and the exit potential. It is also possible to specify that the rod not be removed from the system at the end of one axial transit, and thus, multiple reflections of the beam at the end space may also be simulated. An account of the cumulative power dissipation on the circuit due to insertion loss is also kept.

Electron stream reentrancy through the drift space is handled by taking the charge remaining in the interaction space at the end of the first pass through the delay line and rearranging the charge rods in pairs. These are then reintroduced at the input to the interaction system for a succeeding pass. They are arranged so that the new radial position of each pair of electrons is the average position which these two rods occupied at the termination of the succeeding run. Thus they enter for the succeeding pass with the total potential of the charge cluster unchanged. However, the phase of these reentering electrons is scrambled so that no RF information remains on the reentering stream. Several iterations of this process may be carried out to simulate reentrancy.

The need to simulate the reentrant feature is of importance only in the case where the ratio of circumferential and axial velocities is such that almost all of the circuit length is traversed during one axial pass, in which case many electrons are still in the system at the end of the first pass. This was indeed the situation during early design estimates, when it was felt that a given electron would pass 17" of circuit length before being removed from the system. However, during later calculations, a more realistic average of 8" of circuit length was used. At the end of the first pass, very few of the charge rods remaining in the interaction space had enough "life expectancy" left to avoid collection during the trip through the drift space. Thus a totally insignificant number of rods would have been reintroduced

for a second pass, and a single pass was adequate to perform the calculations even though reentrancy was permitted. A description of the general results for the calculations with no end reflection follows.

The beginning calculations for the design of this tube were based on an initial estimate that an electron entering the interaction space would traverse about 17" of circuit before exiting. However, a detailed analysis of the differential and axial velocity between the outer and inner edge of the electron beam in the interaction space indicated that this low an axial velocity was not possible. The details of this analysis are presented in Section 2.4. However, the results of this analysis showed that the best that might be achieved was to have the axial velocity of the inner or lower edge of the beam set at about 10 electron volts. The axial velocity of the upper or outer edge of the beam would correspond to about 50 electron volts. This means that the top electron would traverse about 4.6" of circuit length before exiting, while the bottom electron would traverse about 10.5", so that an average electron in the middle of the beam might traverse about 8" of circuit legnth before exiting.

In the discussion of the computer runs which follows, the quantity FRACLN is the length of circuit traversed circumferentially during one axial transit in the manner just described. The results of three sets of large signal runs done for three different values of FRACLN are discussed below. The three values are 17", representing almost a complete revolution for one axial transit; 8", the mean value for the more exact situation; and 5", the value for the top edge electron in the beam. The results of these various runs indicate the great sensitivity of tube performance to this value of FRACLN, particularly when the value drops to a small fraction for the total circuit circumference.

In order to calculate the efficiency from the various large signal runs, it was presumed that the six collector elements had the following potentials (with respect to cathode potential) applied to them.

Collector Element	Potential
1	290 v
2	1390 v
3	2490 v
4	3590 v
5	4690 v
6	5800 v

The computer output includes the distribution of exit potentials for the various electrons entering the collector system. Thus each exiting charge rod can be assigned to one of six appropriate collection potentials and the conversion efficiency calculated for the actual six-element collector to be used in the tube. In addition, the potential distribution makes it possible to calculate a limiting value of efficiency that will be obtained if there were an infinite number of collector element; i.e., the collection voltages are continuous.

Figure 7 gives the results of the computer run for FRACLN equals 17". Although this is not a realistically achievable value, it is included here to show the manner in which tube performance is dependent upon this value of FRACLN. This run is the only one discussed in this report that was made for a cathode current of 1 ampere. All other runs were made at the revised design value of 1.8 amperes.

The results of this first run are plotted in Figure 7. The RF power along the circuit is plotted as a function of distance along the circuit in wavelengths measured from the end where the RF drive is applied. This is the only value of FRACLN of the various runs for which a sufficient number of charge rods remained at the end of the first pass to require repeated iterations. The results shown are the end of the second iteration for a drive level of 20 watts and a frequency of 300 MHz. RF output power is 2941 watts corresponding to 21.68 db of gain. A histogram showing the fraction of the exiting beam current going to each collector element is shown in Figure 8.

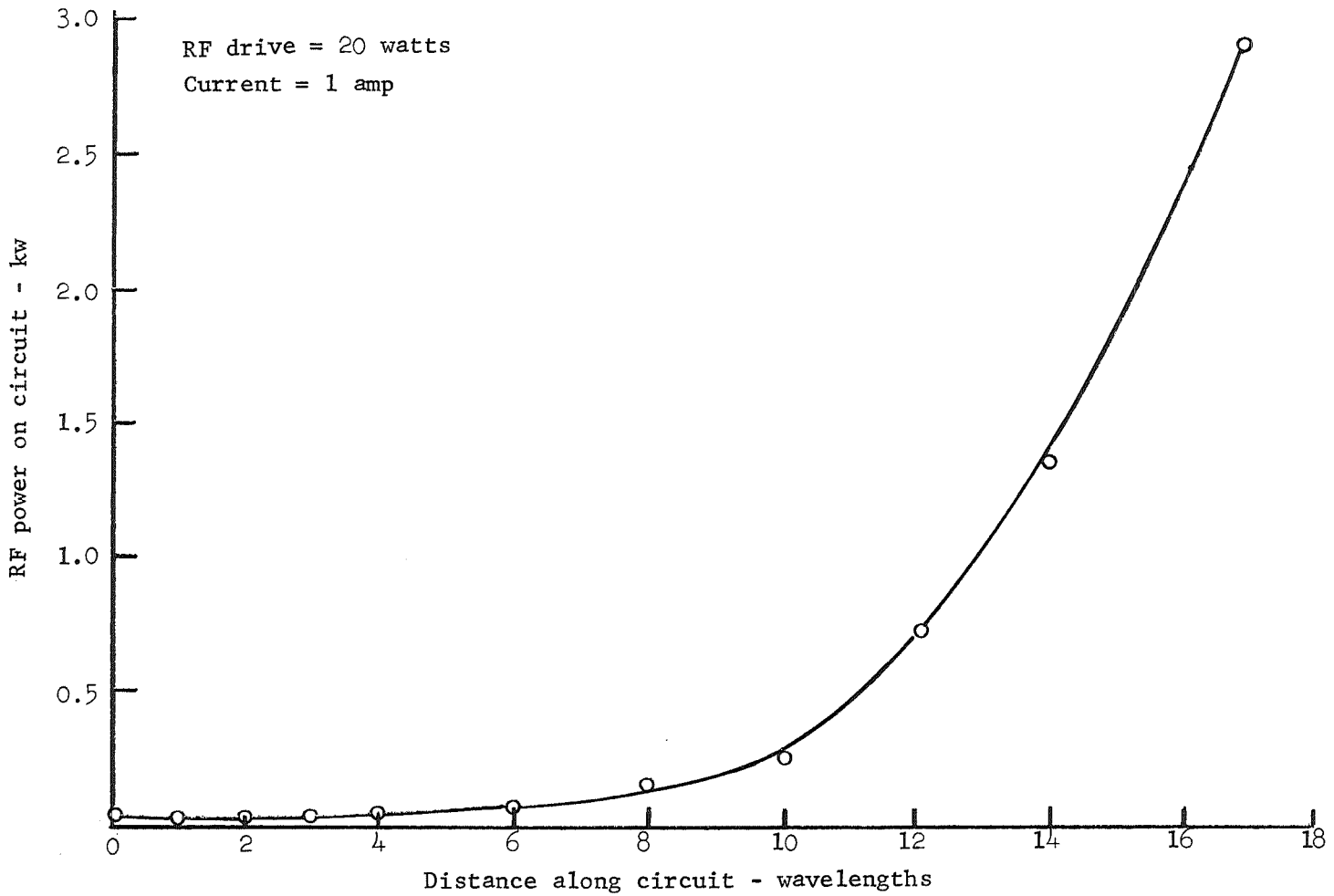

FIGURE 7 COMPUTER SIMULATION OF AMPLIFIER PERFORMANCE FOR FRACLN = 17"

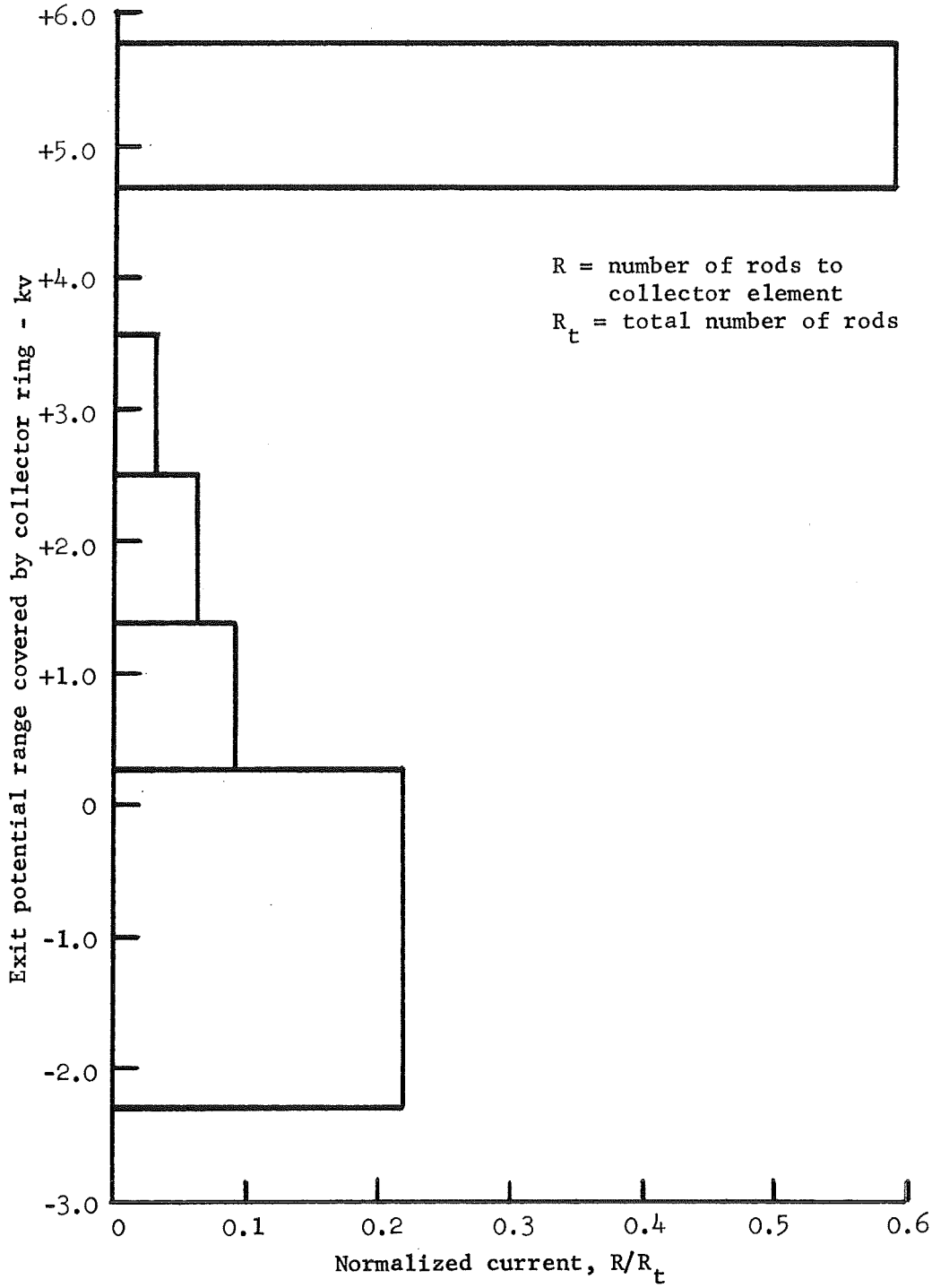

FIGURE 8 DISTRIBUTION OF CURRENT VERSUS COLLECTOR POTENTIAL FOR CONDITIONS OF FIGURE 7

This current distribution results in an estimated conversion efficiency of 79%. The limiting value for an infinite number of collector elements would be about 90%.

Succeeding runs were made based on more realistic values of the parameter FRACLN. Figure 9 is a plot of RF power along the circuit and gain level, again as a function of distance along the circuit from the input end. The RF drive level is 20 w and the current level is 1.8 amperes, which is the final design value of cathode current that was chosen for this system of operation. It is seen that the tube is not quite driven to saturation at 20 w of drive. Figure 10 is a histogram of the current distribution in the spent beam as a function of exit potential. Based on this current distribution the conversion efficiency at this drive level with the six-element collector is 46.5%, while the asymptotic efficiency for a system of continuous collection voltages would be 69.7%. Supplementary studies carried out under the previously referenced NASA Lewis study program indicated that at a drive level of 60 w, a conversion efficiency with the six-element collector of 63% was achievable.

The next two runs cover the case of a FRACLN of 5" corresponding to an axial velocity equivalent to about 60 electron volts which would be the axial velocity of the top electron in the beam when the bottom electron has an axial velocity corresponding to 10 electron volts. The deterioration in performance under these conditions is substantial. Furthermore, for the first time, a distinct difference from small signal gain calculations is observed. Small signal gain calculations have been carried out for the conditions of these various large signal runs by taking the circulating current as being equal to 1.8 amperes multiplied by the ratio of FRACLN to the actual total circuit length. In this case, for FRACLN = 5", the circulating current for the small signal calculation was taken to be 0.34". This resulted in a calculated small signal gain of 22 db. The

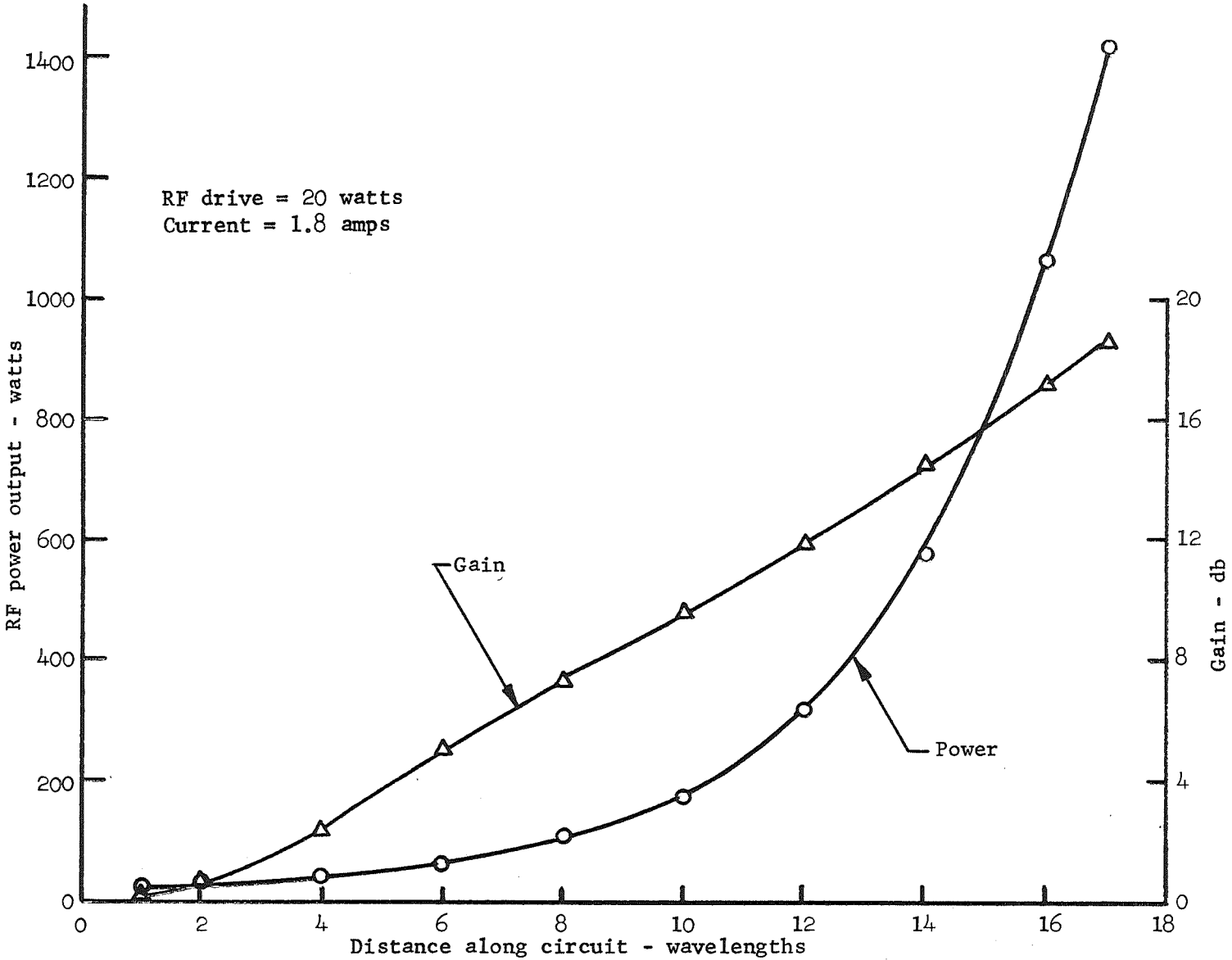

FIGURE 9 COMPUTER SIMULATION OF AMPLIFIER PERFORMANCE FOR FRACLN = 8"

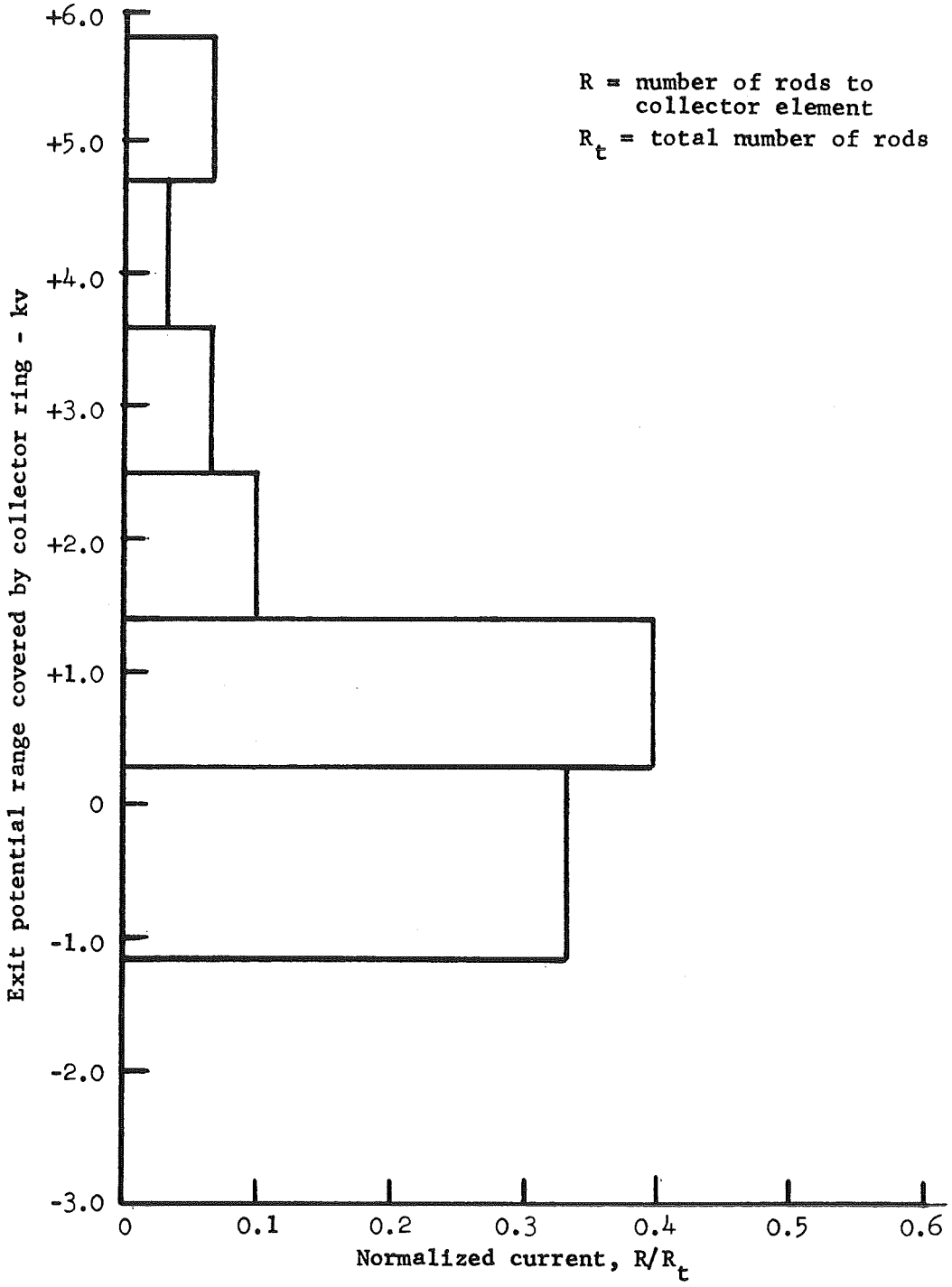

FIGURE 10 DISTRIBUTION OF CURRENT VERSUS COLLECTOR POTENTIAL FOR CONDITIONS OF FIGURE 9

results of the large signal run are shown in Figure 11. At 20 w of RF drive, only 122 w of power output are obtained and the gain is down to 7.8 db. The plot of current distribution versus exit potential in the spent beam is shown in Figure 12. An examination of this current distribution shows the large concentration of current at low exit potential, indicating that current is not in the interaction system long enough to move from the injection radius to a position close to the anode and form a current spoke characteristic of large signal interaction. A low value of gain and conversion efficiency are obtained. It is seen that for this very low value of FRACLN, the model set up for calculation of the small signal performance has fallen apart and thus a lower limit for the effective use of this model has been established. At the higher values of FRACLN which were examined, i.e., 8" or more, the small signal gain model correlated reasonably well with the results obtained from the large signal calculations.

In order to determine whether a large value of RF drive would move the electrons more rapidly into a large signal spoke formation, the run for a FRACLN of 5" was repeated for 100 w of drive. The results of this run are plotted in Figure 13. The gain level has been raised slightly to 8 db with a power output of 640 w. The current distribution for this situation is shown in Figure 14. It is of interest to note that even with this very large value of drive, the tube is still not driven into saturation because of the very low value of effective circulating current. The efficiency for the six-element collector, based on the current distribution shown in Figure 14, is 28.2%. The asymptotic efficiency for a collector with an infinite number of elements would be 54%.

The foregoing sequence of large signal calculations has demonstrated the dependence of tube performance upon the effective value of FRACLN. For FRACLN having an average value of about 8", the conversion efficiency of about 46.5% might be expected at 20 w of RF

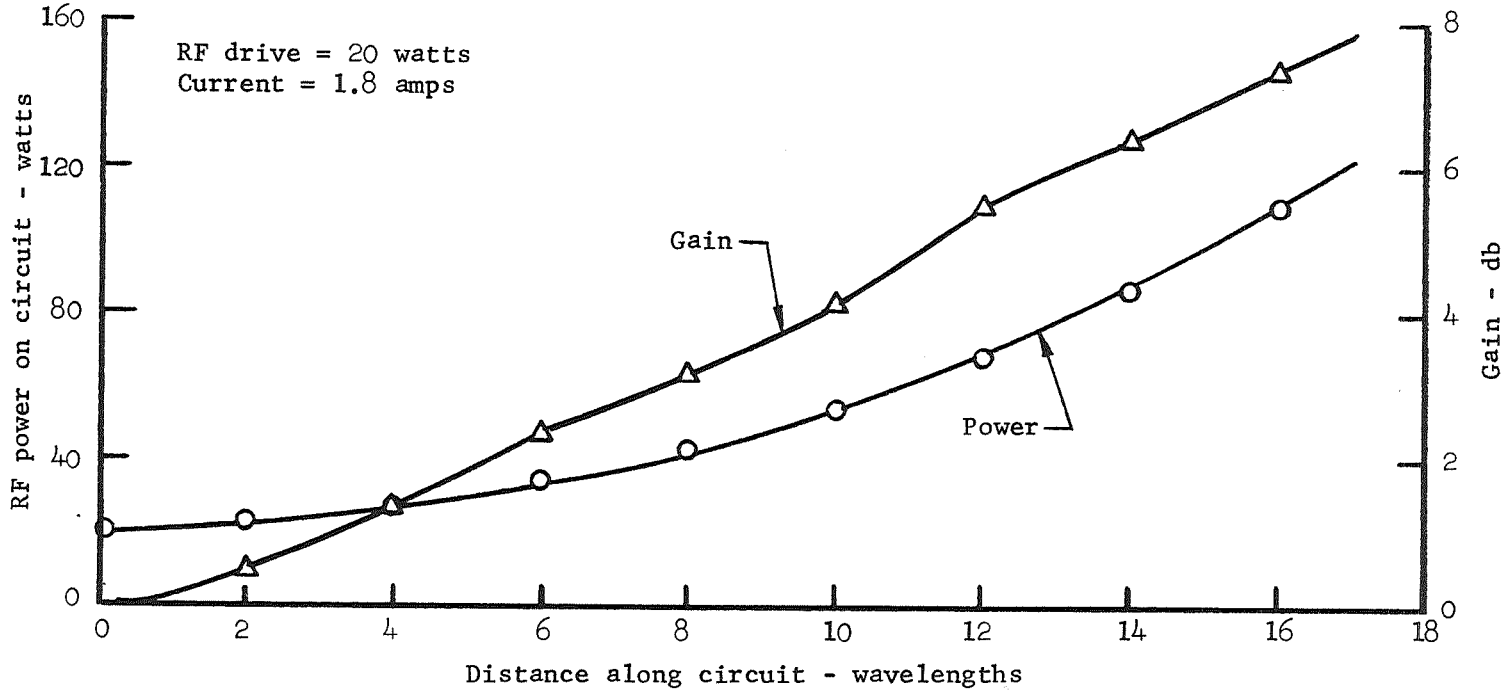

FIGURE 11 COMPUTER SIMULATION OF AMPLIFIER PERFORMANCE FOR FRACLN = 5"

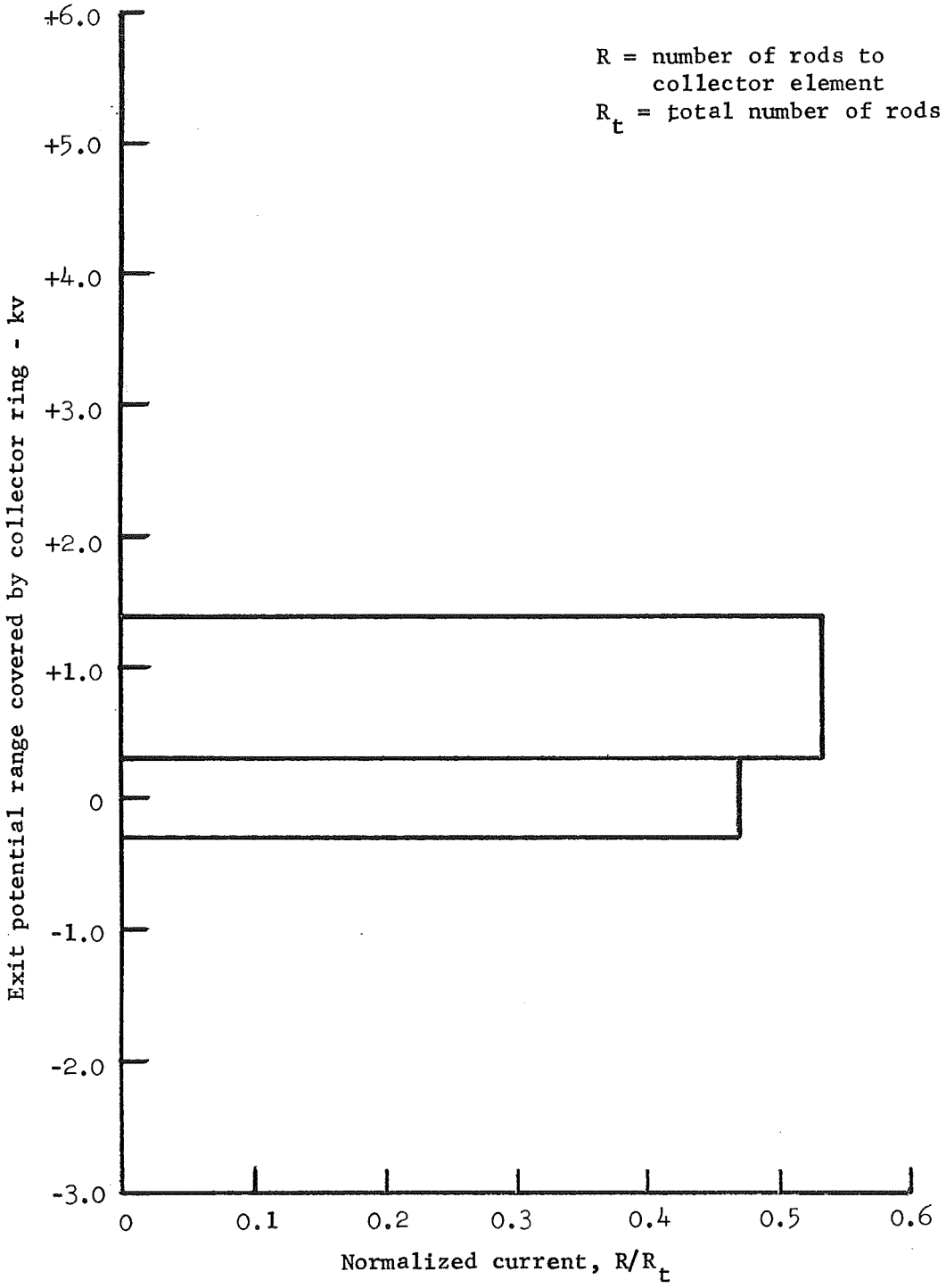

FIGURE 12 DISTRIBUTION OF CURRENT VERSUS COLLECTOR POTENTIAL FOR CONDITIONS OF FIGURE 11

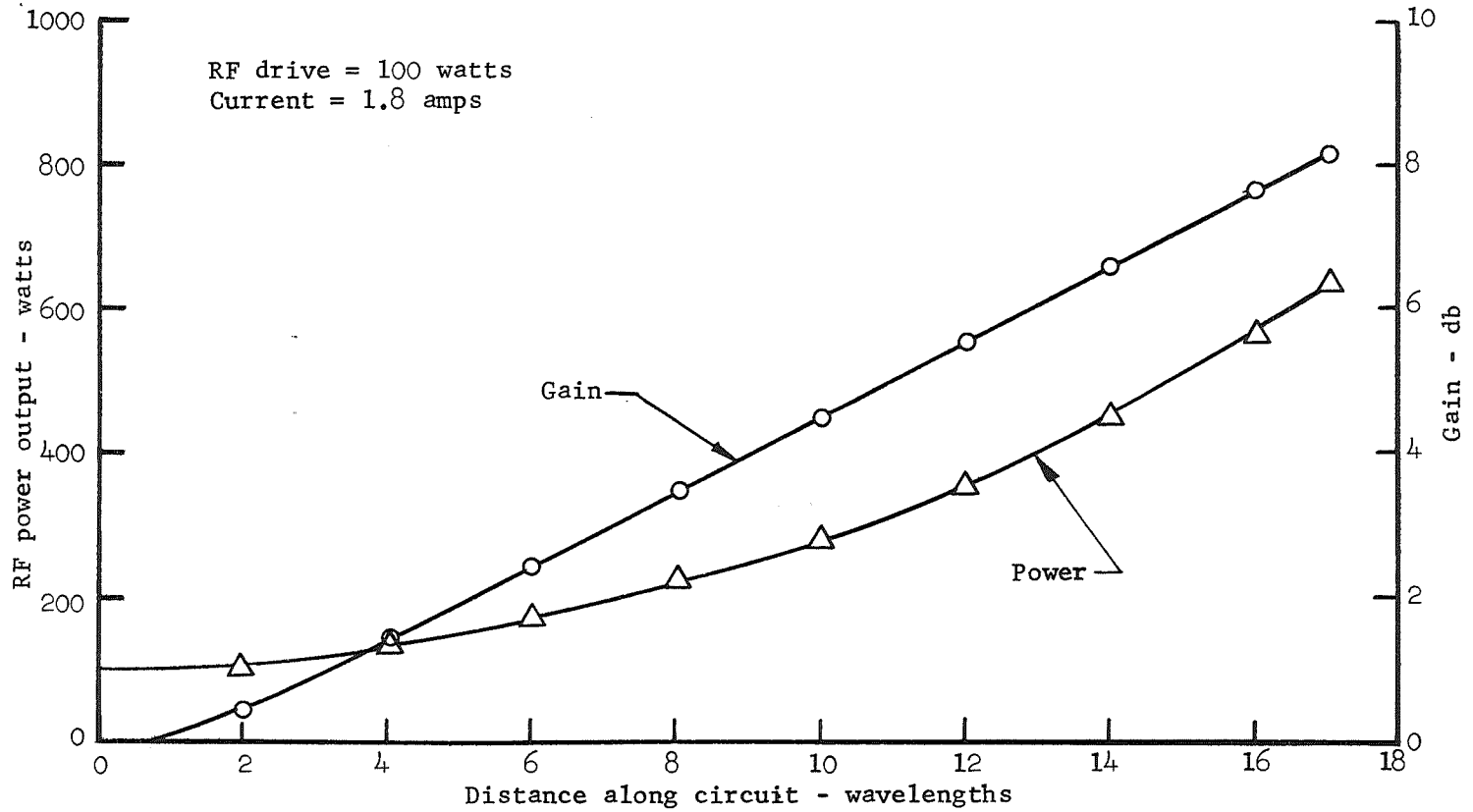

FIGURE 13 COMPUTER SIMULATION OF AMPLIFIER PERFORMANCE FOR FRACLN = 5"

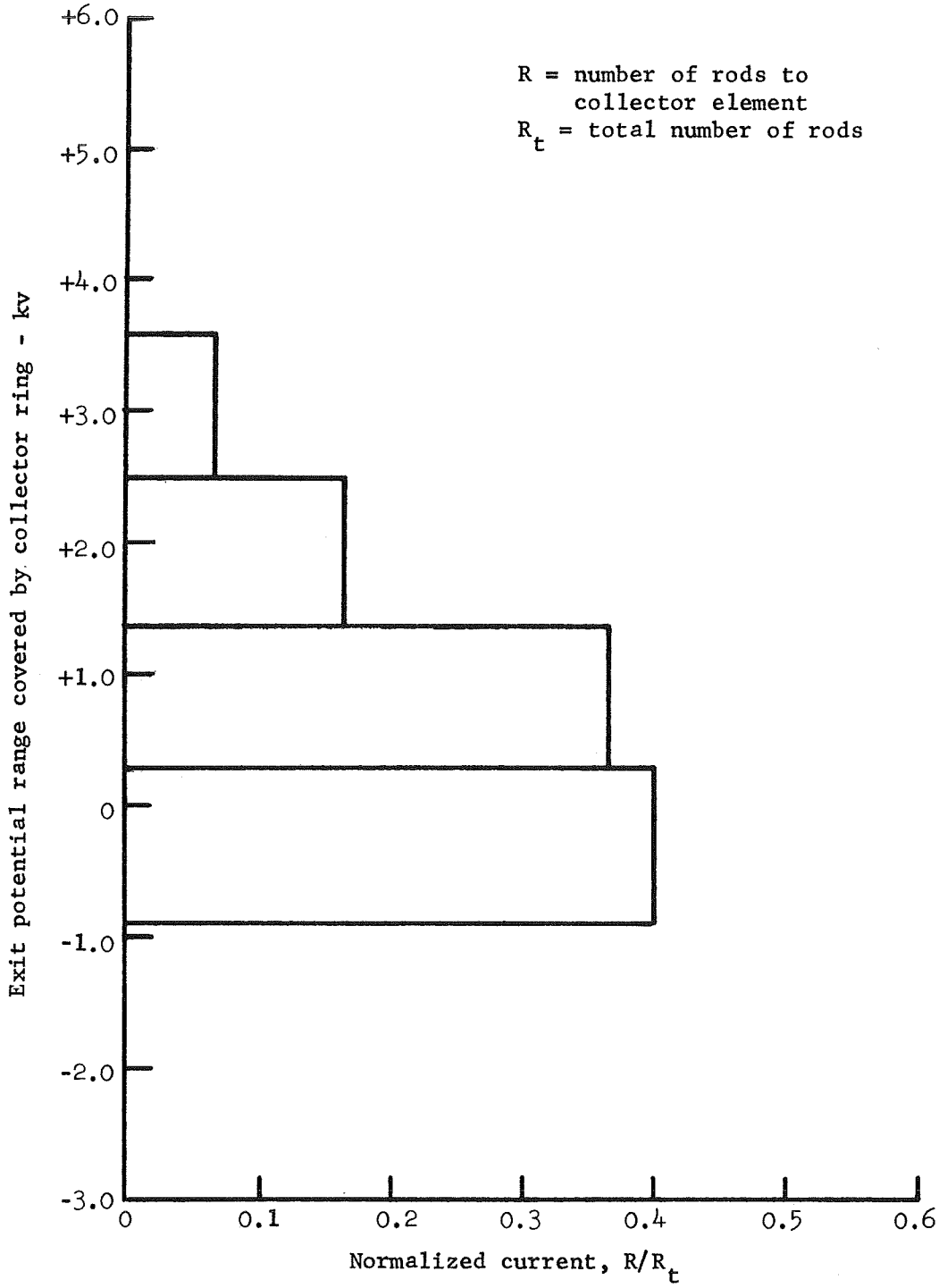

FIGURE 14 DISTRIBUTION OF CURRENT VERSUS COLLECTOR POTENTIAL FOR CONDITIONS OF FIGURE 13

drive. In supplemental studies carried out under the NASA Lewis study program previously referenced, a confirmation of these results was obtained using a more detailed analysis. First, instead of using a single value of FRACLN representing an average for the beam, three velocity classes were actually run. These were FRACLNs of 5", 8.1", and 11.4", corresponding to maximum, minimum, and average values of velocity. The result for 20 w of drive was 19.1 db of gain and a 47% conversion efficiency with the six-element collector, values very close to those obtained with the approximation of a single average value of FRACLN. The same runs using the three velocity classes, again for 60 w of drive, resulted in 17 db of gain and 63% efficiency for the six-element collector. These runs were then repeated with the inclusion of space charge yielding substantially similar results.

Fundamental considerations which will be discussed subsequently limit the mean axial velocity of the beam to about 26 electron volts. Therefore the foregoing series of calculations demonstrate that operation in a mode which allows the beam to exit after one axial transit results in efficiencies with the six-element collector of about 46% with 20 w of drive and about 63% with 60 w of drive. An alternate mode of operation therefore becomes attractive in order to further enhance the value of conversion efficiency obtainable. This mode of operation is indicated in Figure 15b. In Figure 15, the theta (θ) direction along the circuit length is from left to right. Figure 15a demonstrates the electron trajectories for the case where one complete revolution occurs during the time of an axial transit. Current emission occurs from the cathode, which runs the entire circumference of the delay line. However, in situations such as this where a sufficiently low ratio of axial to circumferential velocity is not obtainable, an alternate scheme of operation is needed as shown in Figure 15b.

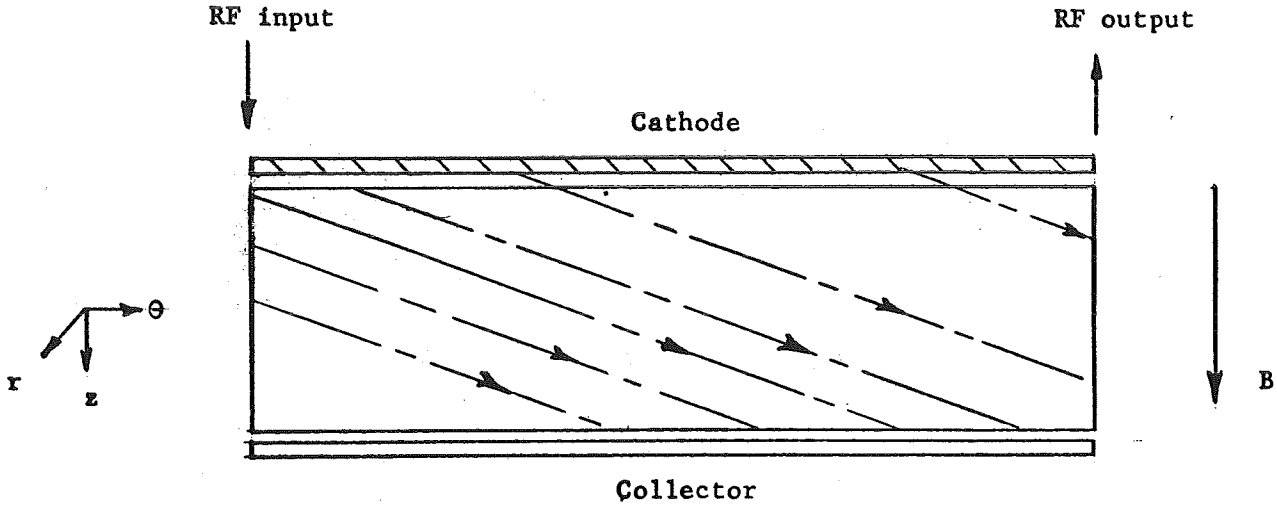

a. One complete revolution during time of axial transit, continuous injection of current

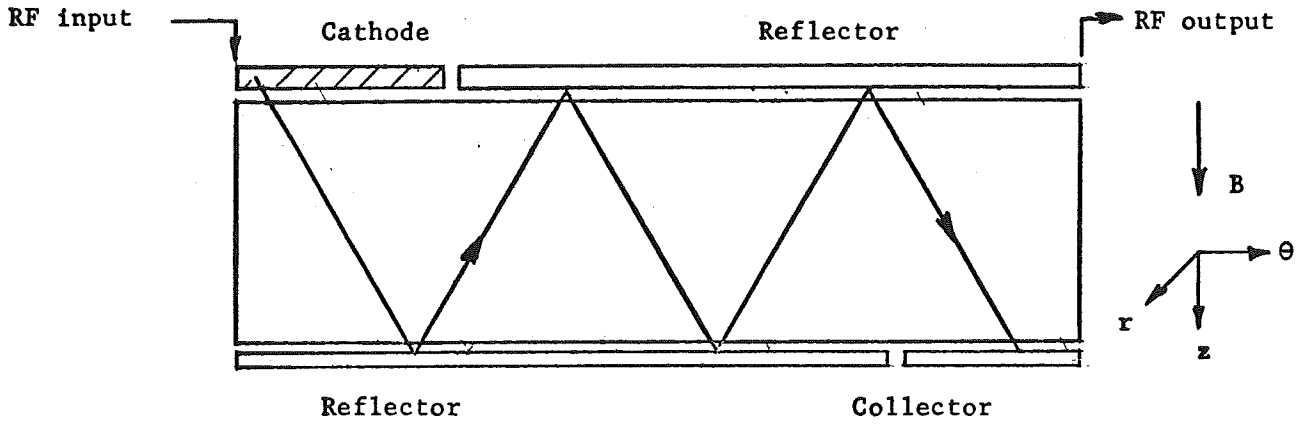

b. Small fraction of a revolution during time of axial transit, current injection along part of circuit

FIGURE 15 ELECTRON TRAJECTORIES SHOWN ON INTERACTION SPACE UNWRAPPED INTO PLANAR VIEW

This sketch covers the case where only a small fraction of a revolution occurs during the time of one axial transit. In order to make more effective use of the current, a reflector replaces the collector system over most of the circuit length. The multi-element collector now exists at a segment of the circuit near the output end or actually in the drift space region. A similar reflector is shown at the cathode end of the interaction space. Thus the electron stream will make multiple transits axially through the interaction system. Since this short circumferential travel effectively eliminates reentrancy (few electrons would get through the drift section), there is no longer any point to injecting the current along the entire length of the circuit. Current injected near the output end would be essentially wasted. Thus the axial injection of current now takes place from a cathode whose length is limited to a fraction of the total of the circuit length, say typically one-quarter or one-third of the circuit length. An additional factor which points to consideration of this approach comes from the experimental results which are discussed later. These results indicate that in order to maintain low noise operation, the reentrancy of the beam should be inhibited. This system of multiple reflection with current injection occurring along the circuit near the input end is capable of giving high efficiency performance while still retaining the current control that accompanies the axial injection scheme. A large signal run carried out under the NASA Lewis study program for the parameters of this tube, using 1 ampere of cathode current and a scheme of reflection as shown in Figure 15b, resulted in an output power of 3250 w with 20 w of drive. This is 22 db of gain and a conversion efficiency for the six-element collector system of 71%, which was quite close to the theoretical asymptotic limit of 76% for an infinite element collector system. This is a result of fully utilizing the cathode current by a system of multiple reflections. These considerations are reinforced by some of

the experimental results discussed later in this report, indicating that a scheme of multiple beam reflections should result in the highest levels of tube performance.

The voltages on the reflector elements need not be set so that total reflection of the beam occurs. The potential on the reflecting elements may be set so that only the electrons which enter the reflection region above cathode potential are reflected. Electrons below cathode potential represent out-of-phase electrons and would be collected and removed from the system, thus giving rise to a greater rate of gain and making possible a shorter circuit length and higher efficiency of operation.

2.4 Design of Electron Gun and Evaluation of Beam Parameters

The magnetron injection gun and transition region into the interaction space are shown schematically in Figure 16. The electron beam is generated in the magnetron injection gun and enters the interaction space, arriving at steady state trajectory such that the average circumferential velocity is equal to the phase velocity of the anode circuit. This fact is assured by proper adjustment of the ratio of electric to magnetic fields in the interaction space. There are two factors of interest in launching the beam. One of these is minimizing the amount of cycloiding performed by the beam about its mean radial position in the interaction space, since this cycloiding represents a component of kinetic energy which may be wasted in dissipation on the anode delay line for the collector structure.

The other item of interest is the difference in axial velocity between the outermost edge of the beam and the inner edge of the beam. This velocity differential sets the minimum value at which the upper edge of the beam may travel. When the upper edge velocity is equal to this differential, the lower edge velocity must be zero and the beam is at the point of being stopped and reflected back into the gun region.

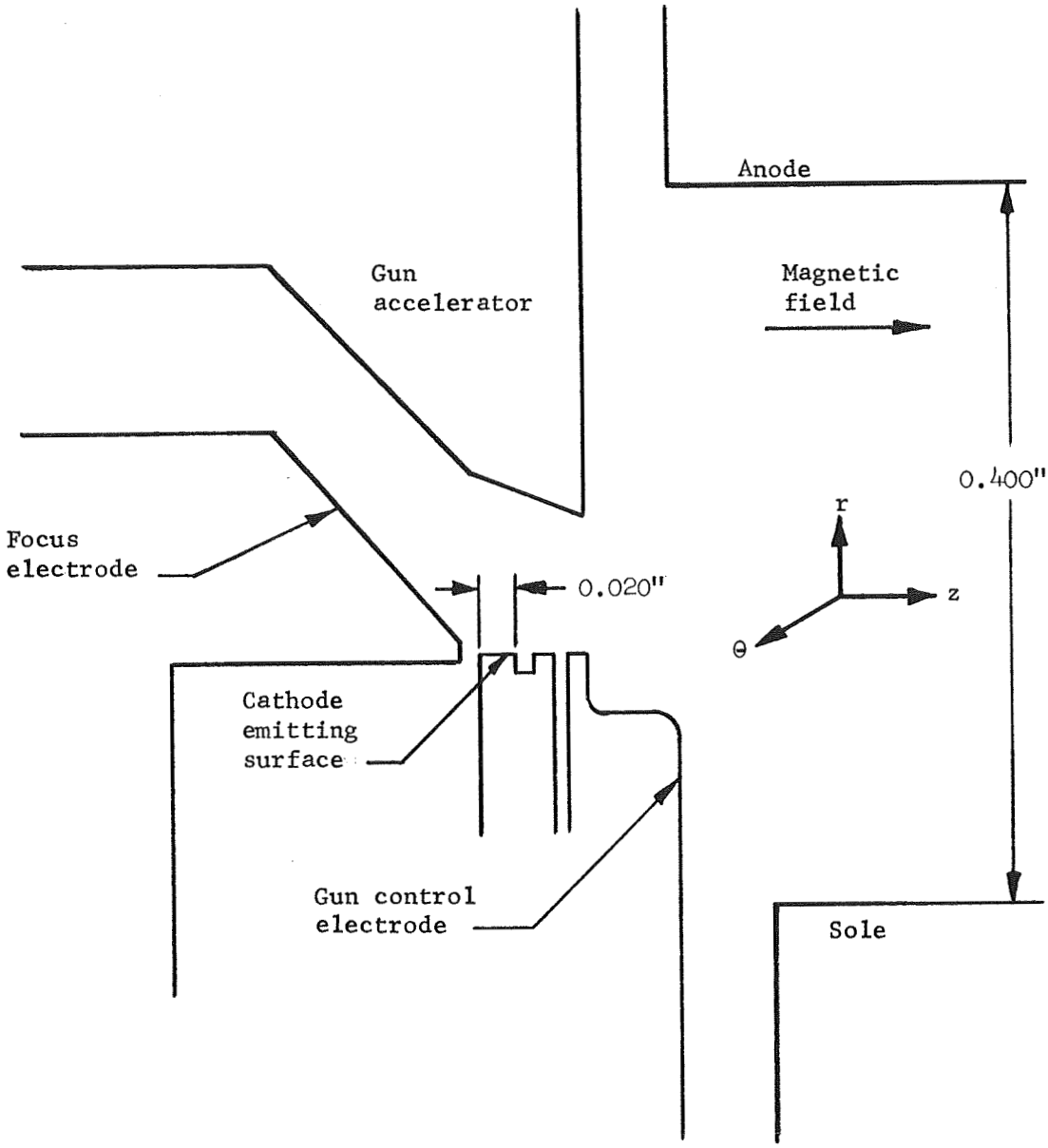

FIGURE 16 MAGNETRON INJECTION GUN AND TRANSITION REGION TO INTERACTION SPACE

It will be shown that the differential in axial velocity is set by factors which involve the thickness of the beam, the current, the magnetic field, and the geometry of the gun. It is possible to vary the mean value of beam axial velocity by the adjustment of voltages on those electrodes which affect electric field in the transition region between the electron gun and the interaction space.

A computer program which has been developed to do trajectory tracing for the axial injection beam was used to establish the degree of control which the sole bias can exercise over the mean axial velocity of the electron beam. This program was also used to evaluate the degree of cycloiding to be expected under the launching conditions set up by the gun design.

It was shown in Section 2.3 that the performance of the tube is dependent upon the parameter FRACLN which represents the length of circuit traveled by an electron during one axial transit. It was further asserted that this distance expressed as a fraction of the total circuit length is equal to the ratio of circulating current to cathode current in the small signal model of the axial injection amplifier. This relationship of currents is derived in Figure 17. When the electron beam has been launched and has entered the interaction space, there is a differential in both the circumferential velocity and the axial velocity between the top and bottom edges of the beam. The slip in the circumferential velocity is set by the space charge conditions in the beam. The slip in axial velocity is set by the electron gun design parameters and the details of the field encountered by the electron beam in the transition region between the gun and the interaction space. As will be shown, this differential in axial velocity is actually dependent only on the terminal conditions in the interaction space and the cathode tilt angle. A lower limit on the axial velocity is reached when the axial velocity at the bottom of the beam is reduced to zero and the top of the beam has an axial velocity equal in magnitude to this differential.

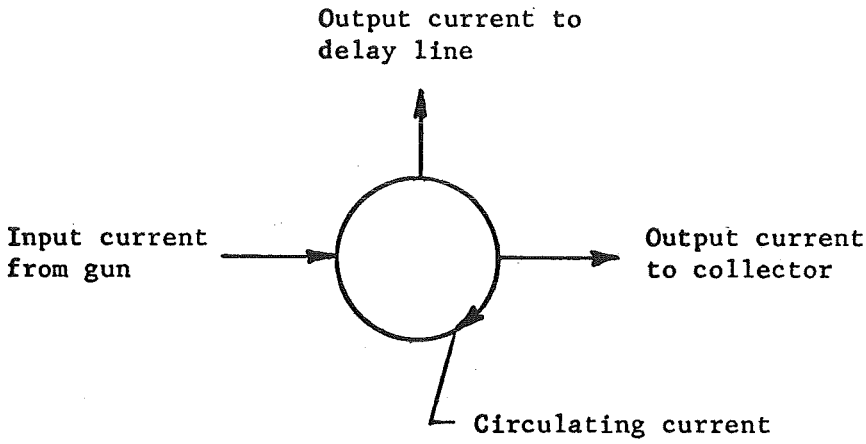

a. A symbolic representation of input, output and circulating currents

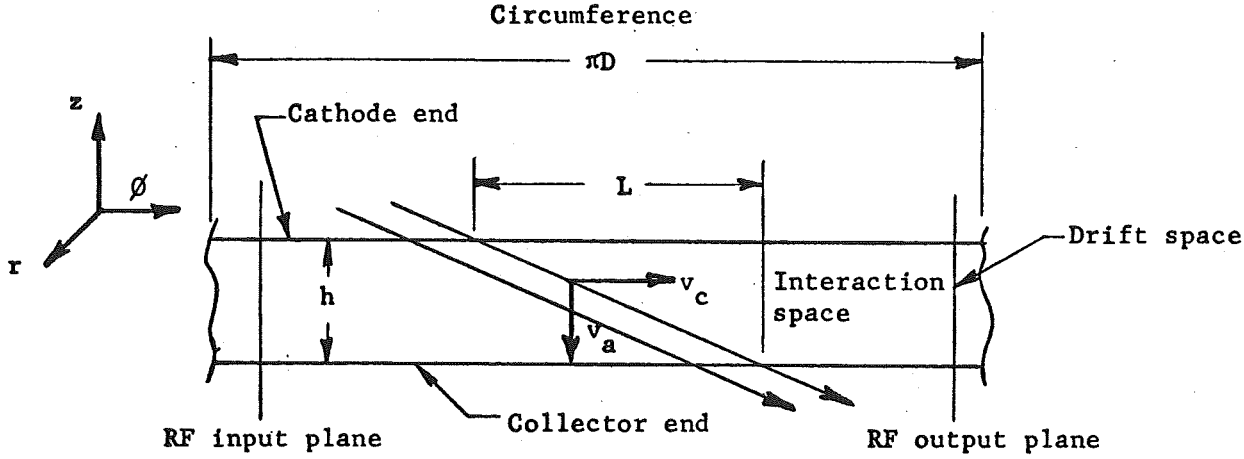

b. Unwrapped view looking down from anode toward unwrapped interaction space

Each electron has circumferential and axial drift velocities, v_c and v_a respectively. Let ρ_o be the space charge density in the beam under low level conditions when the beam is uniform throughout the interaction space and let t be the beam thickness in the radial direction (out of the paper). The circumferential current is then $\rho_o thv_c$ and the axial current is $\rho_o t\pi Dv_a$ where D is the beam diameter on injection. The ratio of these currents $I_c/I_a = (h/\pi D)(v_c/v_a)$. However h/v_a is the transit time t for an electron through the interaction space and $v_c t = L$ is the circumferential distance an electron travels while in the interaction space. Thus $I_c/I_a = L/\pi D$ or the ratio of circumferential to axial current is equal to the fraction of the full circumference that a trajectory covers in its traverse across the interaction space.

FIGURE 17 INPUT, OUTPUT, AND CIRCULATING CURRENTS

These are the conditions under which the beam is just on the verge of being reflected back into the gun region. However, the mean value of axial velocity for the electron beam can be adjusted by the details of the field seen in the transition region. The sole-cathode voltage is one of the parameters which may be varied to achieve this control.

The design of the magnetron injection gun starts with the Kino analysis (Ref. 2). This analysis is used to establish the conditions in the beam at the exit from the gun region. At this point there is a slip in the circumferential velocity and in the axial velocity between the top and bottom edges of the beam. These quantities are functions of the magnetic field, the cathode tilt angle, the current density, and the length of the cathode. The cathode tilt angle of 4 degrees was chosen for this design since there is some accumulated theoretical and experimental evidence to the effect that maintaining a finite tilt angle is useful in reducing the amount of noise generated within the gun. Physically this means that the current is removed rapidly from the gun region before an excessive buildup of noise can occur.

Therefore, although the use of a smaller cathode tilt angle does reduce the differential in axial velocity, these noise considerations led to the choice of an operating angle of 4 degrees. The Kino analysis is also used to design the shape of the accelerator electrode for a particular value of accelerator potential. The parameters of this particular gun design are given in Table III.

As can be seen, the circumferential velocity at the exit plane from the gun is considerably less than the synchronous velocity of 290 electron volts in the interaction region. Thus in the transition region, the radial electric field is increased, increasing the circumferential velocity and also imparting an additional slip in axial velocity between the top and bottom of the beam.

The calculation of axial velocity slip in the interaction space can be carried out by making use of some general relations which

TABLE III

ELECTRON GUN PARAMETERS USING KINO ANALYSIS

Cathode current	1.80 amps
Current density	0.56 amps/cm^2
Magnetic field	900 gauss
Cathode tilt angle	4 degrees
Cathode circumferential length	25.0 in
Cathode area	3.23 cm^2
Cathode width	0.020 in

Velocities and Radial Displacements
of Top and Bottom Edge Electrons from their Points of Origin
Two Cathode Lengths from Corner of Emitting Surface

Two cathode lengths = 0.040 in

	Top Electron	Bottom Electron
θ, inches	0.123	0.077
r, inches	0.0194	0.0145
z, inches	0.0400	0.0200
θ-velocity, electron volts	123.6	77.9
r-velocity, electron volts	1.32	1.00
z-velocity, electron volts	33.6	13.3
Radial electric field, volts/0.001 inch	15.1	

have been derived (Ref. 3) for an axial injection beam having Brillouin flow characteristics in the circumferential direction. The result of this calculation shows that the final differential in axial velocity between the two edges of the beam can be given in electron volts as follows.

$$\Delta v_z = E_o t_k$$

where Δv_z = the differential in axial velocity in electron volts
E_o = the radial electric field at the center of the beam
t_k = the vertical rise of the cathode, i.e.,
t_k = the cathode length multiplied by the sine of the cathode tilt angle

Thus, it appears that the differential is dependent only on the terminal conditions in the interaction space and the initial conditions at the cathode in the gun. The history of the beam in the transition region sets the absolute values of axial velocity but not the differential value. This analytical relationship has been cross checked by the specific numerical results obtained from a sequence of computer runs tracing the electron trajectories from the gun into the interaction space.

The foregoing relationship applies as follows. The operating magnetic field is taken to be 900 gauss. The synchronous voltage is 290 volts and the radial electric field corresponding to this is 23.1 volts/0.001 inch. This would be the electric field in the center of the beam if the center plane were assumed to be synchronous with the delay line. Since the cathode length is 0.020 inch and the cathode tilt angle is 4 degrees, the cathode vertical rise is 0.0014 inch. This value multiplied by 23.1 volts/0.001 inch gives, by the criteria just quoted, a differential velocity between the upper and lower edges of the beam of 32.3 electron volts. As has been pointed out, this

calculation is independent of the specific details of the electric field distribution in the transition space between the magnetron injection gun and the interaction region. In a series of runs with the trajectory tracing program in which the field in this region was varied, a differential of about 40 electron volts was established between the upper and lower edges of the beam. This was consistent over a series of runs where the absolute value of the axial velocity of the bottom edge of the beam was varied by a factor of 10; i.e., from about 9 electron volts to 93 electron volts.

A series of runs was carried out to determine the extent to which a variation in the sole bias could control the axial velocity of the lower edge of the beam. Most of this sequence of calculations was carried out on the supplemental study program sponsored by NASA Lewis Research Center. Referring to Figure 16, the starting point for the calculation was at the exit plane for the magnetron injection gun region. This was taken to be two cathode lengths beyond the left corner of the cathode as sketched in this figure. The initial constants for the run were those determined from the magnetron injection gun calculations using the Kino analysis and previously given in Table III. Specifically, the following were the initial constants in the calculation.

Circumferential velocity at starting point	
Top	125 electron volts
Bottom	78 electron volts
Axial velocity at starting point	
Top	34 electron volts
Bottom	20 electron volts
Circumferential velocity in interaction space	289 electron volts

Anode potential with respect to cathode	5.8 kv
Sole potential with respect to cathode - variable	~ -3.4 kv
Gun accelerator potential with respect to cathode	1250 v
Electron gun focus element potential	Cathode potential
Sole-anode spacing	0.4 in

A series of runs was made where the sole voltage with respect to cathode potential was varied in 50 volt steps from -4.0 kv to -3.2 kv. At the higher values of bias voltage, the entire beam was reflected into the gun region. At 3.4 kv, the bottom edge electron was reflected and the top edge electron entered the interaction space. At 3350 v, the entire beam entered in the interaction space with the bottom edge electron having a velocity of 51.5 electron volts. With 22.4 in of active circuit length, these velocities correspond to a FRACLN for the top edge of 4.6 in and a FRACLN for the bottom edge of 10.6 in, with an average value of 7.56 in. It is based on this set of values that the large signal runs using an average FRACLN of about 8 in were initially carried out. Further reductions in bias resulted in increased axial velocities so that at 3.2 kv bias, the lower beam edge electrons were traveling with 93 electron volts and the upper edge electrons were traveling with 132 electron volts. Note that the differential of 40 electron volts is still maintained.

Generally then, one may expect that an axial injection amplifier with this mode of operation will exhibit a variation of cathode current versus sole bias voltage as sketched in Figure 18. This assumes that all other operating voltages and the magnetic field remain constant. When the sole potential is varied in the direction of increasing the negative sole bias, a rapid decrease in current may be expected as the knee of the curve is passed, since various portions

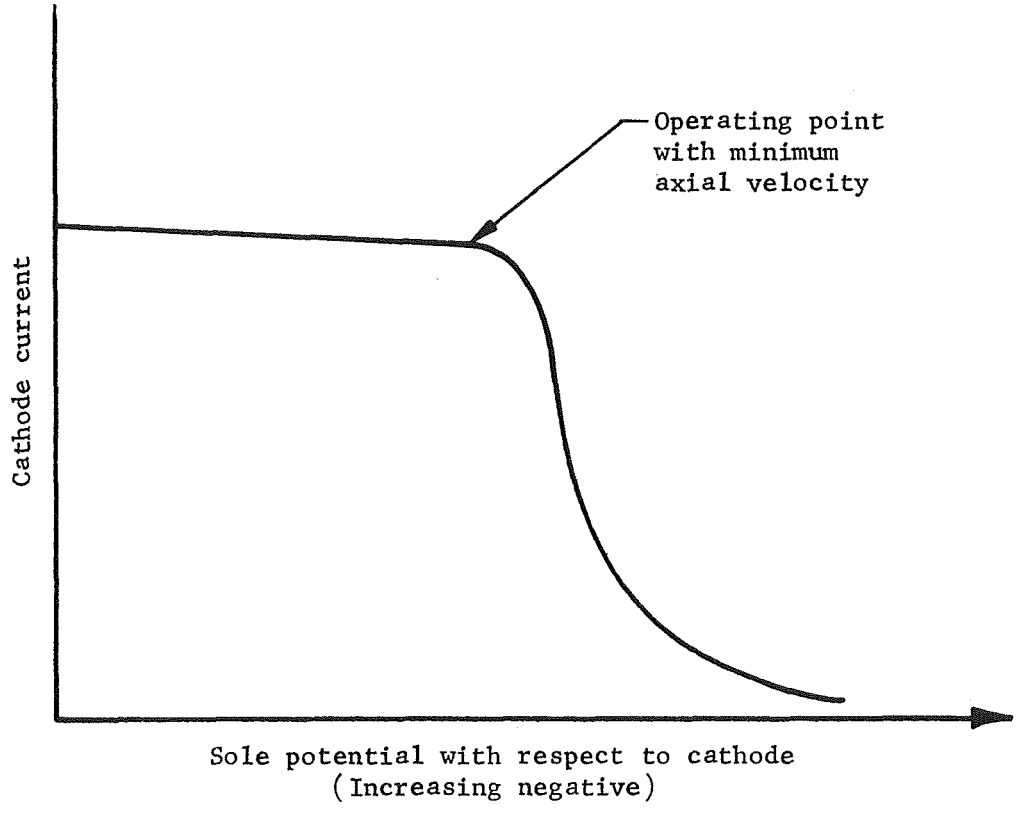

FIGURE 18 CATHODE CURRENT VERSUS SOLE BIAS VOLTAGE

of the beam are reflected back into the gun region. Finally even the most energetic electrons are returned to the gun. Thus, operation at a sole bias slightly less than that appearing at the knee of the curve will insure that the electron stream enters the interaction region with a minimum forward axial velocity, assuring the largest possible value of FRACLN. This particular current characteristic is a diagnostic tool for setting up the operating conditions in an experimental amplifier and determining the operating conditions within the beam.

An examination of the electron trajectories once inside the interaction space showed that for the geometry sketched in Figure 16 with the applied voltages indicated, the beam was smoothly launched. The amount of radial cycloiding corresponded to excursions of about plus and minus 50 electron volts or about 20% of the synchronous voltage. These numbers represent a smooth beam with an unimportant fraction of the total dc input existing in cycloiding energy of the electron stream.

A schematic of the multi-element collector structure is sketched in cross section in Figure 19. The sketch is done in the r-z plane with the axis of symmetry of the tube below the view of the sketch. The sketch is shown to scale with the sole-anode spacing indicated as 0.4 in. The collector elements, labeled 1 through 6, are circular and the bevel shown on the upper righthand side of each collector element is placed there to shape the potential lines in that region so that secondary electrons that might be emitted from the next higher collector element would be returned to the element of emission.

Collector ring No. 1 was divided into four insulated quadrants so that differing voltages could be placed on collector ring No. 1 as a function of circumferential distance along the delay line. One object of this mode of construction was to allow for an experimental assessment of velocity distributions in the electron stream by

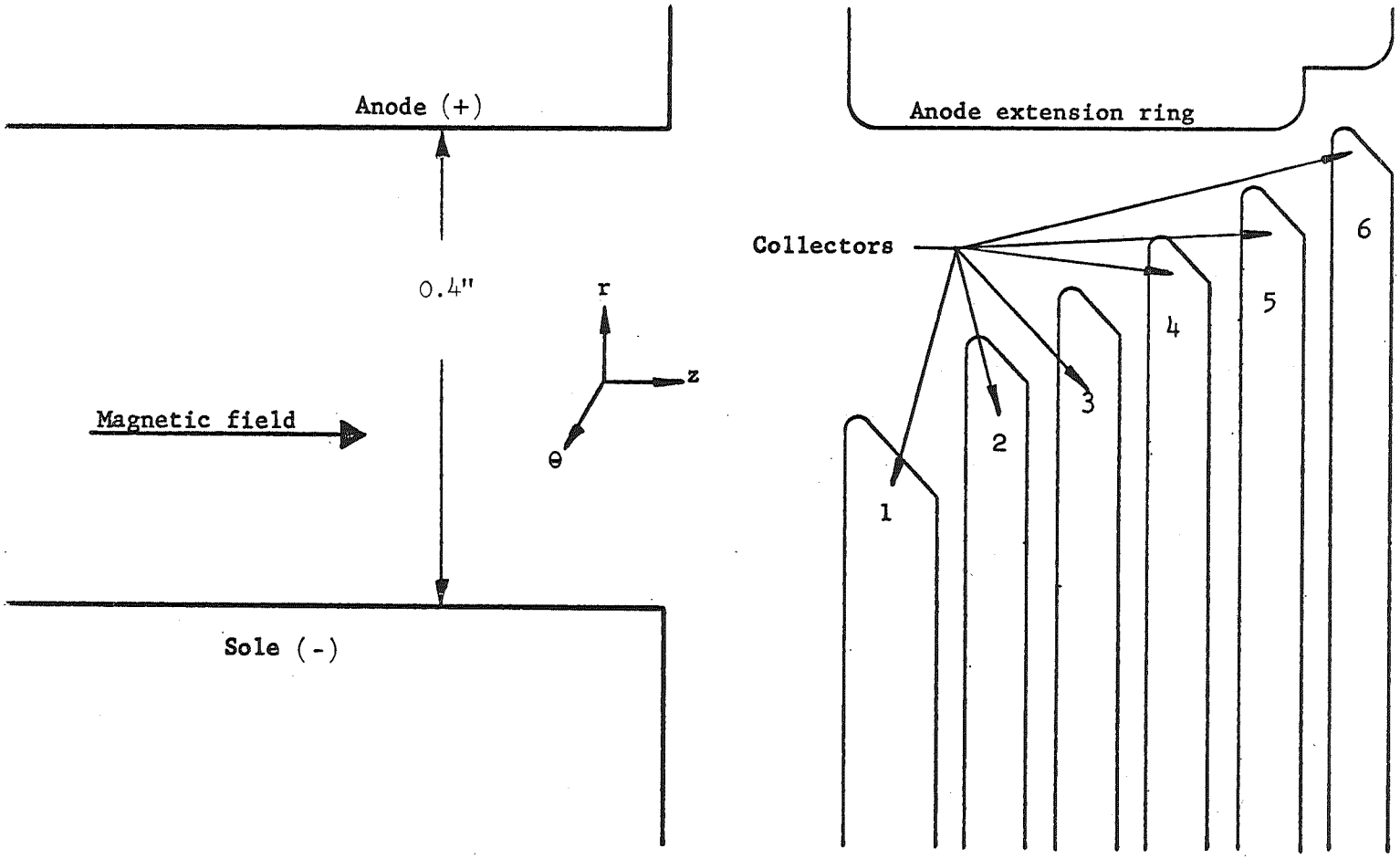

FIGURE 19 SCHEMATIC OF COLLECTOR SECTION

measuring the amount of current collected on the various quadrants of the first ring. In addition, experiments in partial reflection could be carried out by running some of the quadrants of ring No. 1 at potentials which were negative with respect to the cathode. The quadrant of ring No. 1 near the RF output would be set at normal collecting potentials so that partial reflection of the beam would occur along the length of the circuit with collection occurring at the entrance to the drift region near the output end. As already indicated, the normal distribution of voltages on the collector rings in order of increasing radius was as follows.

Ring	Potential
1	600 v
2	1390 v
3	2490 v
4	3590 v
5	4690 v
6	5800 v

The element labeled "anode extension ring" is a smooth bore metallic ring placed in the position indicated to extend the anode potential from the edge of the delay line to collector element No. 6 in a smooth fashion. The spacing between this anode extension ring and the circuit bars of the anode was chosen so as to avoid excessive capacitive loading of the anode bars by the extension ring. After some of the experimental results had been evaluated, it appeared in retrospect that this spacing had been made too large. Further analysis of the collector region carried out with the trajectory tracing program indicated that an excessive distortion of the dc electric field pattern was occurring in the region of the gap between the anode and anode extension ring. This consisted of a bulging of the potential lines into the gap between these two circuit elements resulting in a

potential barrier which electrons traveling axially in this region had to pass through. In Section 3.0 which discusses the experimental results, it is indicated that the collector structure did not function properly, with one of the anomalous characteristics of this malfunction being excessively large amounts of current drawn to the anode extension ring element. Two groups of trajectory tracing runs were carried out in the collector region. These computer runs were done under the analytical design program sponsored by the NASA Lewis Research Center. The first group of runs took a cluster of seven electrons and allowed them to enter the collector region from the interaction space with radial positions corresponding to a potential distribution which varied from -1100 v to +5340 v with respect to cathode potential. Their axial velocity toward the collector structure corresponded to 50 electron volts. The results of this run showed that only the three lowest potential electrons, that is those at potentials below 1.2 kv, reached their appropriate collector rings. The four electrons that had been injected at the higher potential positions were all reflected back into the interaction structure. Examination of the potential plot that the program produces showed that a 200 v potential barrier existed in the region of the gap between the anode and anode extension ring. Subsequent runs which attempted to minimize this effect by varying the potential of the anode extension ring did not produce appreciably different results.

A second set of runs was carried out to investigate the paths of electrons generated by secondary emission at the collector rings. Secondary emission electrons were simulated by placing a series of electrons just in front of the surface of the various collector elements. The electrons were given a few electron volts of axial velocity toward the interaction region as well as in the direction of increasing radius. The electrons at the lower potential collector rings reentered the interaction space where they would rejoin

the main electron stream. However, the electrons at the highest values of potential were turned back and driven into the ring of next higher potential, increasing the effective dc power input. Thus it is felt that the distortion introduced by this oversized gap between the two elements in the collector region is an important factor in the malfunctioning of the collector structure and in the apparently ineffective performance of the collectors.

3.0 THE EXPERIMENTAL AMPLIFIER AND TEST RESULTS

The amplifier whose design has been described was assembled for testing in a solenoid, so that experimental flexibility could be maintained by allowing a variation in magnetic field. A photograph of the assembled amplifier is shown in Figure 20. The assembled RF impedance transformers are seen in the photograph. These connect the input and output ends of the anode delay line to external 50 ohm transmission lines. These transformers are external to the vacuum envelope of the tube. The helix loaded bar circuit which constitutes the anode of the amplifier has a surge impedance of approximately 300 ohms. The transformer consists of a small length of helix loaded bar circuit in which the bar and coil dimensions are varied in a series of steps. The ratio of unit inductance to unit capacitance of the artificial transmission line is reduced from a ratio yielding a surge impedance of 300 ohms to a ratio yielding 50 ohms. This reduction is done in a manner which keeps the inductance-capacitance product essentially constant so that the cutoff frequency and dispersion characteristics of the equivalent filter network are the same as for the delay line itself. The transformers are connected through the vacuum wall to the delay line at the high impedance end by a short length of two-wire transmission line that enters through the top plate as shown. This arrangement results in added experimental flexibility for this tube. The tube is assembled by a system of heliarc welds, making it possible to open up the electron gun end or collector end for further design modifications of the experimental vehicle.

Further experimental flexibility was obtained in this amplifier by having two additional control elements inside the tube. These consist of gating electrodes in the drift tube section - one flush with the anode surface, the other flush with the sole surface. These two electrodes run essentially the entire axial height of the

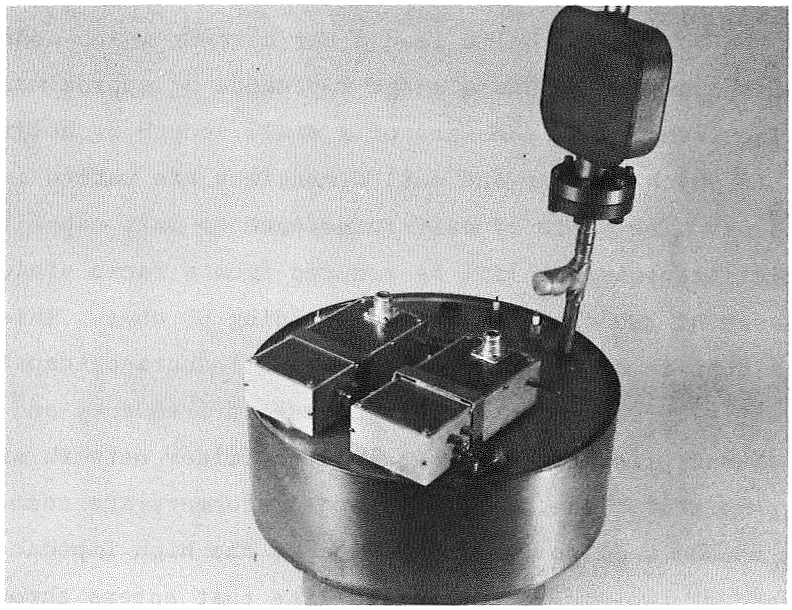

FIGURE 20 PHOTOGRAPH OF ASSEMBLED UHF AMPLIFIER

delay line and are insulated so that negative or positive voltages, with respect to the sole or anode structures, can be applied to them. These elements were used in the experimental work to evaluate operation of the amplifier under conditions where reentrancy was inhibited. This turned out to be a necessary condition for eliminating background RF noise in the absence of RF drive.

The circular heater for the ring cathode was divided into separate insulated sections. The first section was a quarter circle in length and was at the input end of the delay line, while the other three-quarter circle of heater covered the remaining arc of the cathode. This was done to provide still further experimental flexibility so that parts of the cathode could be turned off while runs were being made.

It had been agreed that in order to obtain a maximum of performance information before evaluating the thermal capabilities of the tube, the initial round of RF test measurements would be done on a pulsed basis. Thus, the initial measurements were carried out at a 0.001 duty cycle. This was done by applying the appropriate dc potentials to the various elements of the tube but with the accelerator maintained at a negative voltage with respect to cathode potential so as to keep the gun from emitting. During the "on" time, a positive pulse was applied to the accelerator electrode to bring the gun into conduction. The RF drive pulse was made about twice as wide as the applied voltage pulse so that the tube came on and went off during the time of the RF pulse.

Initial runs were made using the entire cathode circle for emission, with no attempt to reflect the beam back from the end spaces. In the discussions that follow, all voltages are called out with respect to cathode potential. In order to avoid some voltage standoff problems that arose, the operating cathode-anode potential is reduced from the design value of 5.8 kv to 4.8 kv, leaving the ratio of anode

to synchronous voltage still at a high value of 17 to 1.

It will also be observed that the magnetic field used was somewhat lower than the 900 gauss that was originally used in the 5.8 kv theoretical calculations. The reason for this lies in the fact that when space charge forces were not taken into account, the calculated magnetic field required to make the center of the beam synchronous with the delay line phase velocity was higher than if space charge forces were accounted for. Therefore, for the large signal program and the trajectory tracing routine, 900 gauss is the appropriate magnetic field to establish synchronous conditions when space charge forces are left out. However, when space charge forces are taken into account and the center of the beam is presumed synchronous with the delay line, then the reduction in electric field at the center of the beam results in a reduced value of magnetic field. This reduced value was used in the large signal calculations that took space charge into account. Thus at the theoretical 5.8 kv that was used in the large signal calculations when space charge was considered, the appropriate magnetic field was 818 gauss and a further reduction followed at the actual experimental voltage used, 4.8 kv.

With pulsed amplifier measurements being made at a cathode current of 1.8 amperes, several important factors emerged from the testing to modify the expectations of the original design model. In order to obtain noise free operation, it was necessary to completely inhibit all beam reentrancy. This was done by putting the sole insert at or very close to anode potential. Having eliminated the background noise, the following results then emerged. The gain obtained by operating the tube close to the knee of the sole-bias cutoff curve was close to the value calculated, that is about 20 db. However, the conversion efficiency obtained with the six-element collector structure was considerably below that calculated. There appeared to be two main

reasons for this. One was a malfunctioning of the collector structure so that an excessively large amount of current went to the anode extension ring. This current was collected at full anode potential and did not represent fully interacted electrons. Secondly, the need to inhibit reentrancy by placing the sole insert at anode potential meant that an additional component of current was collected at full anode potential without being fully interacted. These two factors together served to reduce the expected efficiency for non-reflection operation.

Typical performance characteristics under the two sets of conditions just described are shown in Figures 21 through 24. Figure 21 shows a typical sole bias-cathode current curve. The synchronous operating point occurred at just about 1850 v of bias; that is, the operating parameters had been adjusted so that operation would occur just at the knee of the curve.

Figure 22 is a plot of RF power output versus drive power. No attempt is made with this set of operating conditions to inhibit reentrancy. All quadrants of the first collector ring are 600 v positive with respect to cathode potential, with the other rings at the potentials indicated. The curve of signal frequency power output is the output power as measured through a filter tuned to the drive frequency. The total power output is obtained by removing the filter. At the lower levels of drive, the difference between the signal frequency energy and the total energy output is a spectrum of broad band noise. It will be noted that at saturation the conversion efficiency is about 34%, an indication that the six-element collector is not performing properly.

This can be seen from the curves plotted in Figure 23 which shows the anode current and anode extension ring current as a function of RF drive. It is noticed that over the range of drive power, the anode extension ring current remains high, thus representing a block

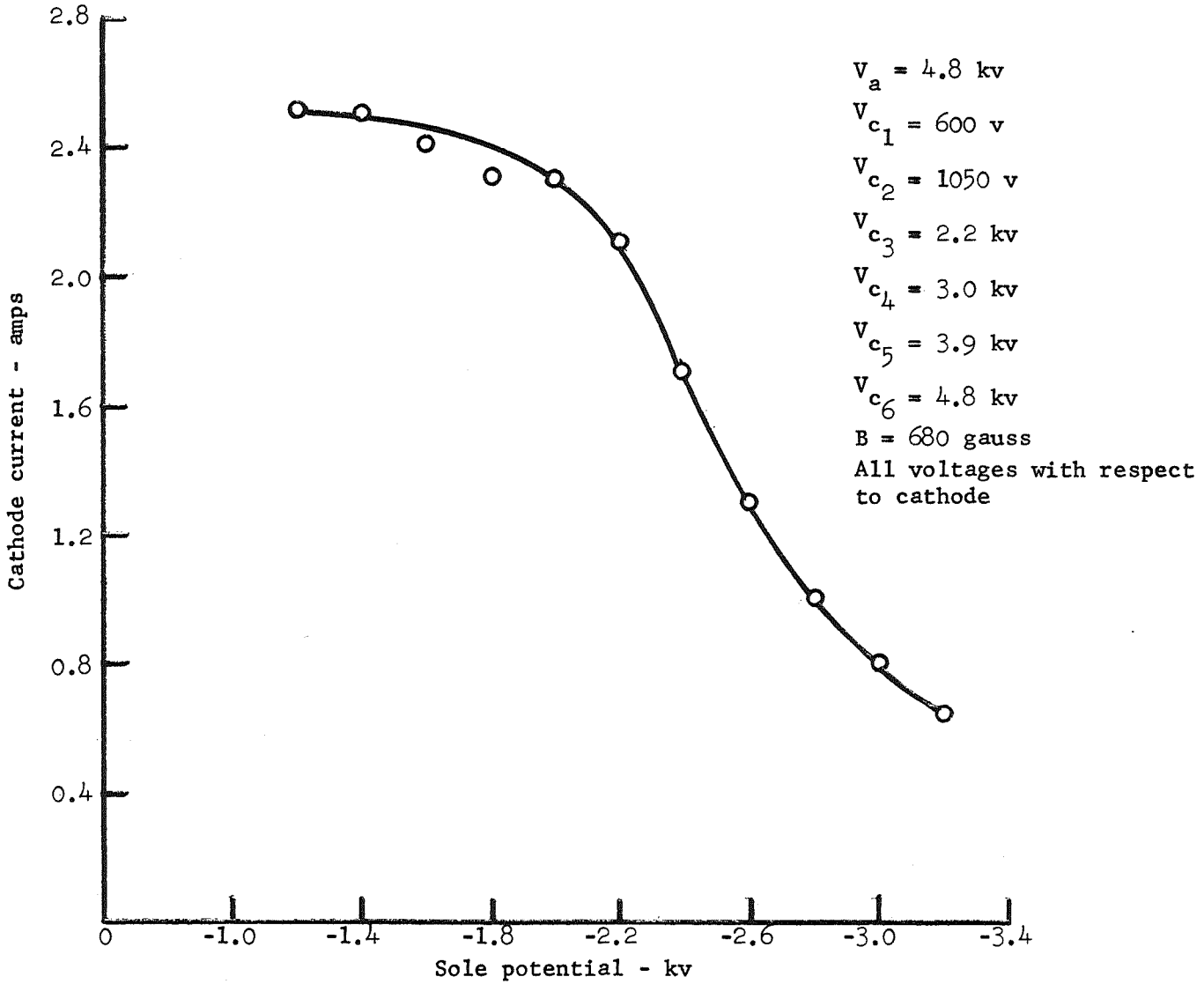

FIGURE 21 CATHODE CURRENT VERSUS SOLE BIAS VOLTAGE FOR UHF AMPLIFIER

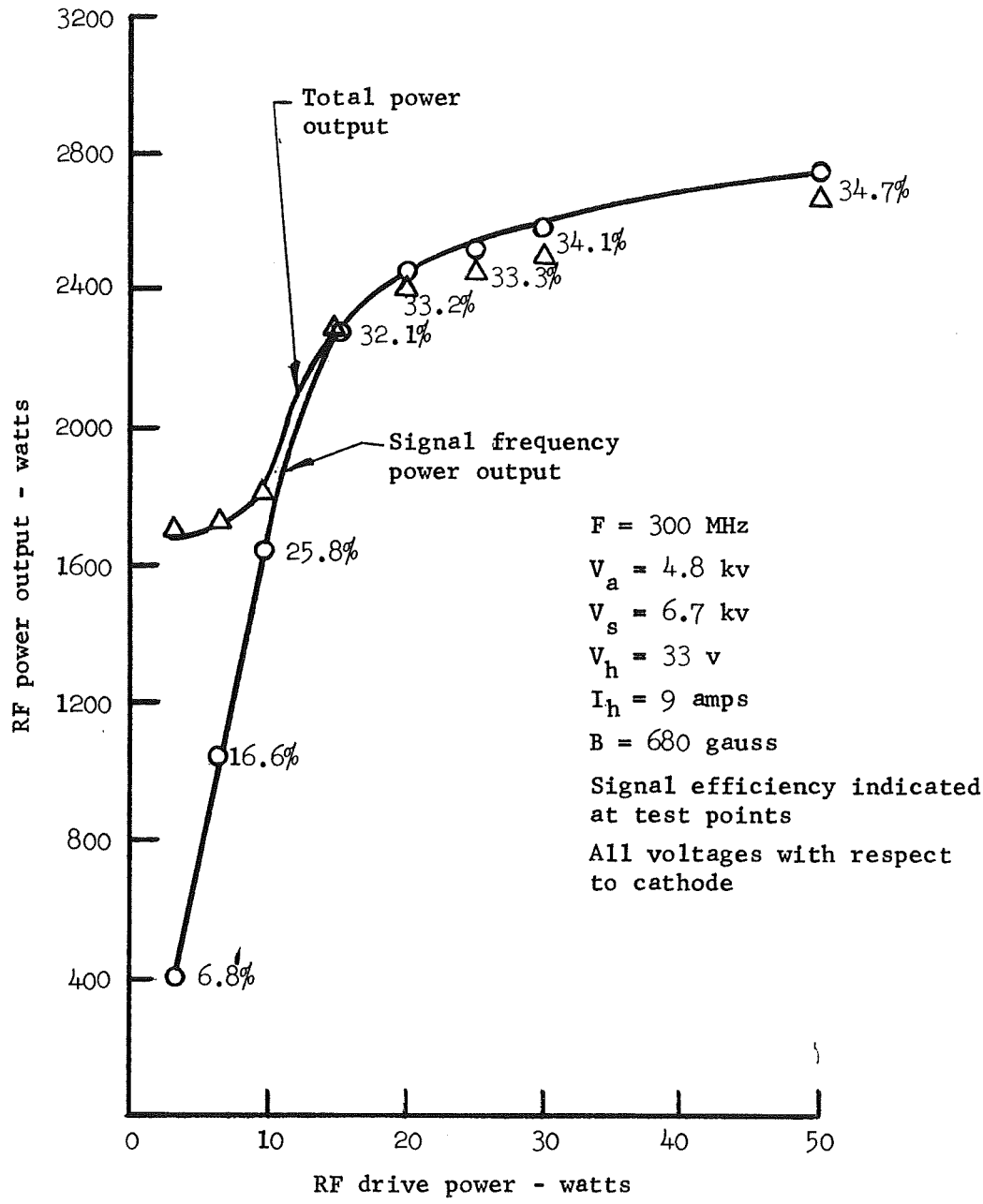

FIGURE 22 PERFORMANCE CHARACTERISTICS OF UHF AMPLIFIER WITH FULL REENTRANCY AND FULL CATHODE EMISSION

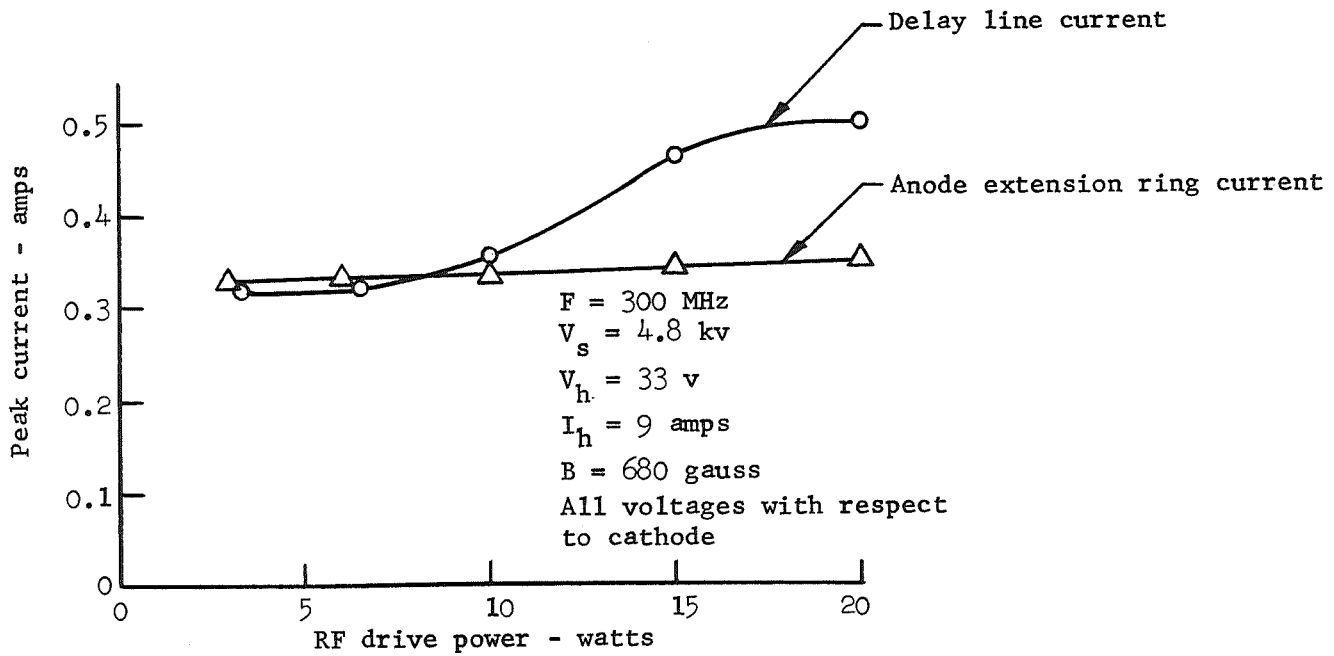

FIGURE 23 DELAY LINE AND ANODE EXTENSION RING CURRENT AS A FUNCTION OF RF DRIVE LEVEL

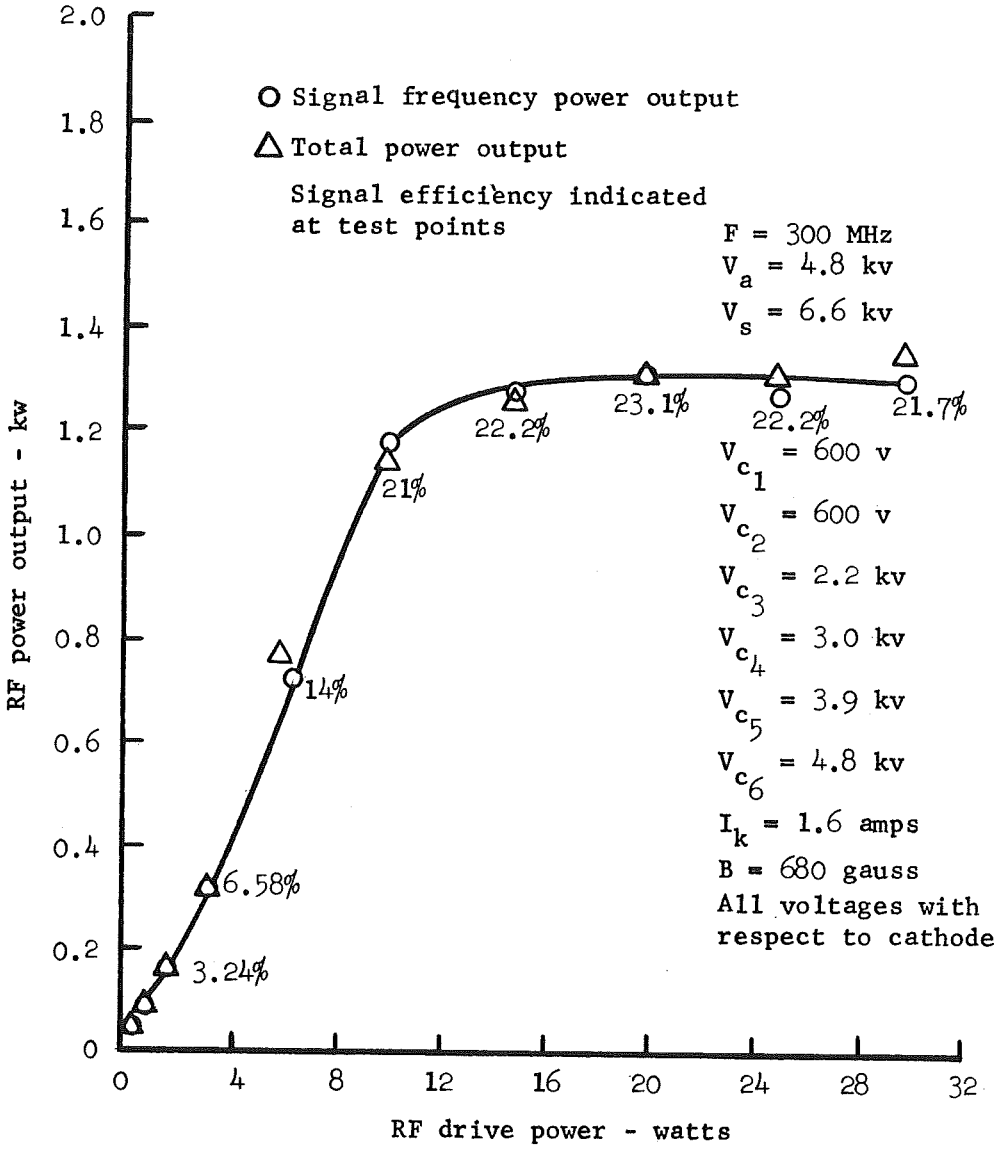

FIGURE 24 PERFORMANCE CHARACTERISTICS OF UHF AMPLIFIER WITH NON-REENTRANT BEAM AND FULL CATHODE EMISSION

of wasted dc input power. The curves of Figure 22 indicate the manner in which the noise energy is locked out as the RF drive level is increased to the saturation level.

When the sole insert electrode is placed at ground potential, thus inhibiting all reentrancy by sweeping electrons in the drift space into this control electrode, the background noise is eliminated as shown in Figure 24. As seen here the conversion efficiency at saturation is about 22% for the power output of 1.3 kw. The small signal gain is still approximately 20 db. The background noise has been eliminated but since the sole insert collects about 20% of the cathode current, the conversion efficiency has been further degraded. The inhibition of reentrancy in this manner, of course, is not the way it would be done if this feature had been originally designed for. The proper way to inhibit reentrancy would be to put a series of in-line collectors in the drift space so that the beam may be collected at the proper potential. Each electron would be collected at approximately the potential which it had when it exited from the interaction space. This would be similar to the present scheme of operation with the end space collector structure.

Recognizing that the collector structure was not functioning properly, it was decided to perform an experiment which would give a measure of the conversion efficiency when the tube was driven to full saturation. This was done by applying sufficiently negative voltage on all of the collector elements, including the anode extension ring, so that no current was collected on any of these elements. The beam was allowed to be fully reentrant in this condition. This is not the normal mode of operation for the axial injection amplifier since with the drive removed under these conditions a large amount of background noise exists. However, when driven to saturation, the noise was locked out. These tests were made at two different levels of RF output power, 1.1 kw and 2.2 kw. The results of these measurements

are given in Figures 25 and 26. It is seen that in the case of the 1 kw run, a saturation efficiency of about 71% was obtained while in the case of the 2 kw run, a saturation efficiency of about 69% was obtained. These runs were made with reduced cathode current - 0.4 amperes in the case of the 1 kw run and 0.8 amperes in the case of the 2 kw run. The reduction in cathode current was made since the collector elements were fully reflecting and the circulating current was equal to the cathode current rather than a fraction of the cathode current. The duty cycle was increased by a factor of 10 to 0.01 to increase the accuracy of the measurements.

The performance characteristics indicated in Figures 25 and 26 were taken with only three-quarters of the full heater circle turned on. This meant that only the three-quarters of the cathode circle which runs along the delay line toward the output port was in operation. Since these measurements were made under a condition of total reflection from all collector rings, it was not necessary to have the full cathode circle emitting. As can be seen, the gain was 20 db and 23 db for Figures 25 and 26, respectively.

It was not possible to carry out a detailed evaluation of performance with the first quarter segment of the cathode circle emitting combined with reflection over the operating length of the delay line, and collection in the drift area near the output port. The reason for this is that the collector structure used here was not primarily designed for this mode of operation. Only ring No. 1 is segmented so that reflecting potentials can be applied over part of its circumference while a proper collecting potential is supplied at the output end. This ring is geometrically placed so as to collect electrons with an exit potential about that of the synchronous voltage. In order to have part of this ring act as a reflector, it is necessary to depress the potential of that ring to nearly sole potential; and it was found that this could not be done without incurring voltage

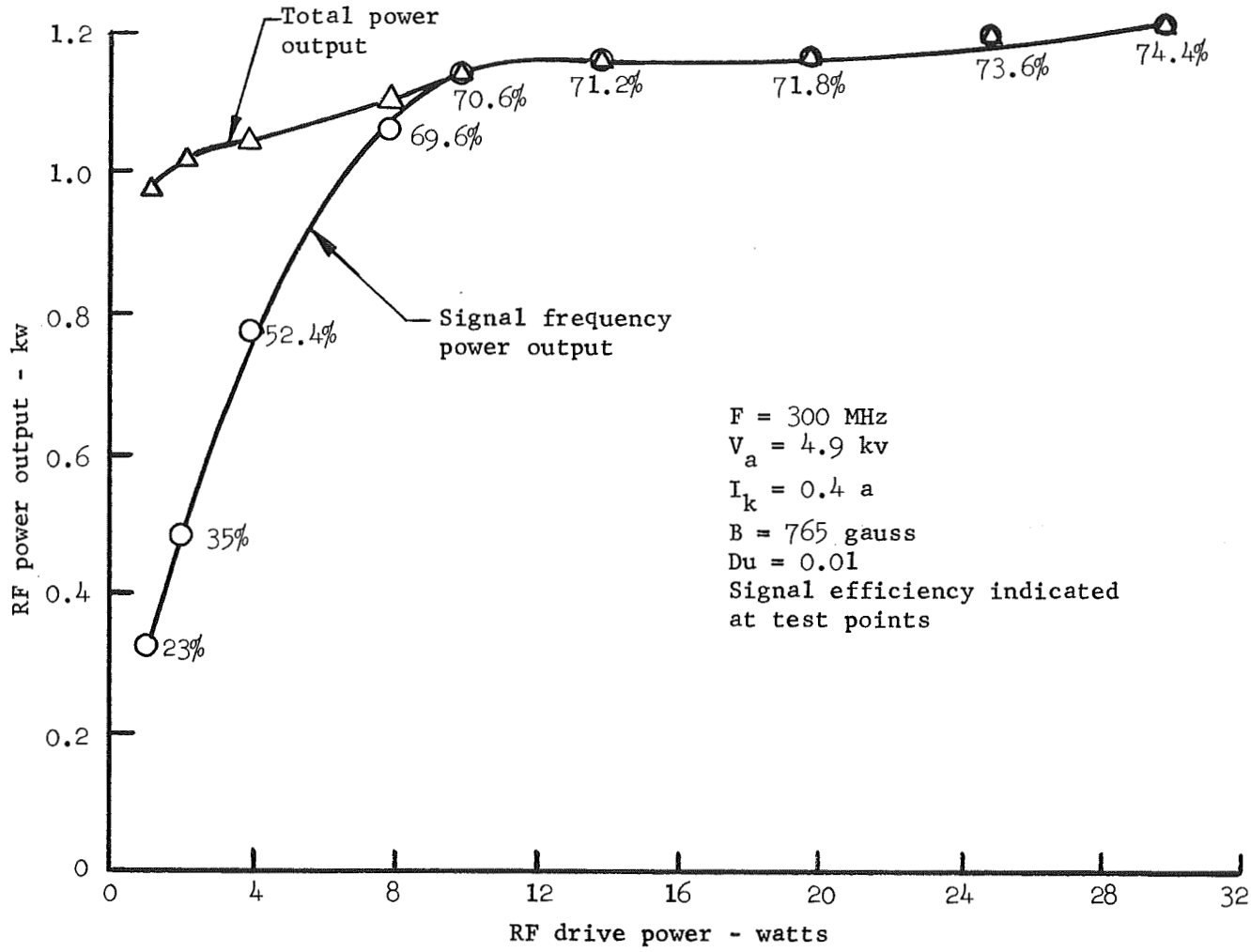

FIGURE 25 PERFORMANCE IN REENTRANT MODE WITH NO CURRENT ON COLLECTOR ELEMENTS, 1 kw LEVEL

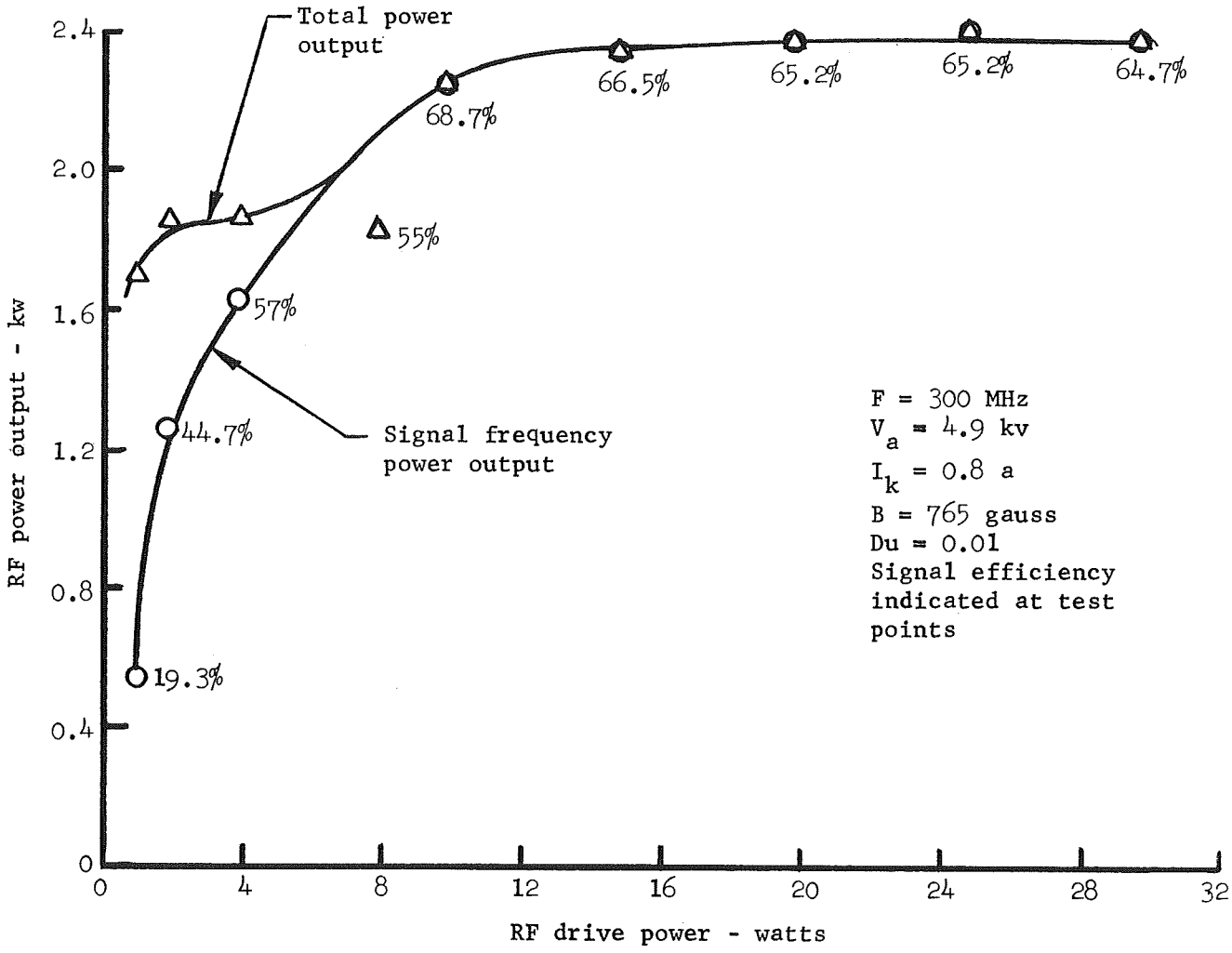

FIGURE 26 PERFORMANCE IN REENTRANT MODE WITH NO CURRENT ON COLLECTOR ELEMENTS, 2 kw LEVEL

standoff problems. Therefore, a complete evaluation of this mode of operation could not be carried out. If the system were designed for this reflection mode originally, then the reflecting element would extend radially to a position much closer to the anode; and a potential either equal to the synchronous voltage or cathode potential would be adequate to reflect most of the beam back into the interaction space. It was found that the elements of the first ring could not be depressed more than about 900 v below cathode potential, and this was not sufficient to give a definitive evaluation of the selective reflection concept.

However, additional experimental evidence does exist to reinforce the validity of the concept involving the use of reflection along the delay line and then collection at the output end. The approach used also involves a blocking electrode which projects from the sole in order to interrupt reentrancy and therefore suppress noise generation. The approach used is not optimal but the performance figures indicate what can be achieved by this scheme. Figures 27 and 28 compare the approach used in this program with the technique used in the other program. Figure 27 sketches the basic collector scheme that was used in the amplifier built on this program. The sole insert as shown was the mechanism used to interrupt reentrancy. Since the insert was flush with the sole itself, it had to be run essentially at anode potential to be effective, thus introducing inefficiency in operation. In addition, the first segmented collector ring was not of the proper geometry to set up reflection of the beam along the delay line. The need to interrupt reentrancy to control noise and the use of electron reflection because of the high axial velocity component lead logically to the concept of using the cathode segment that only runs partially along the delay line.

This scheme has been implemented, as shown in the sketch in Figure 28, in the axial injection amplifier built on the other program

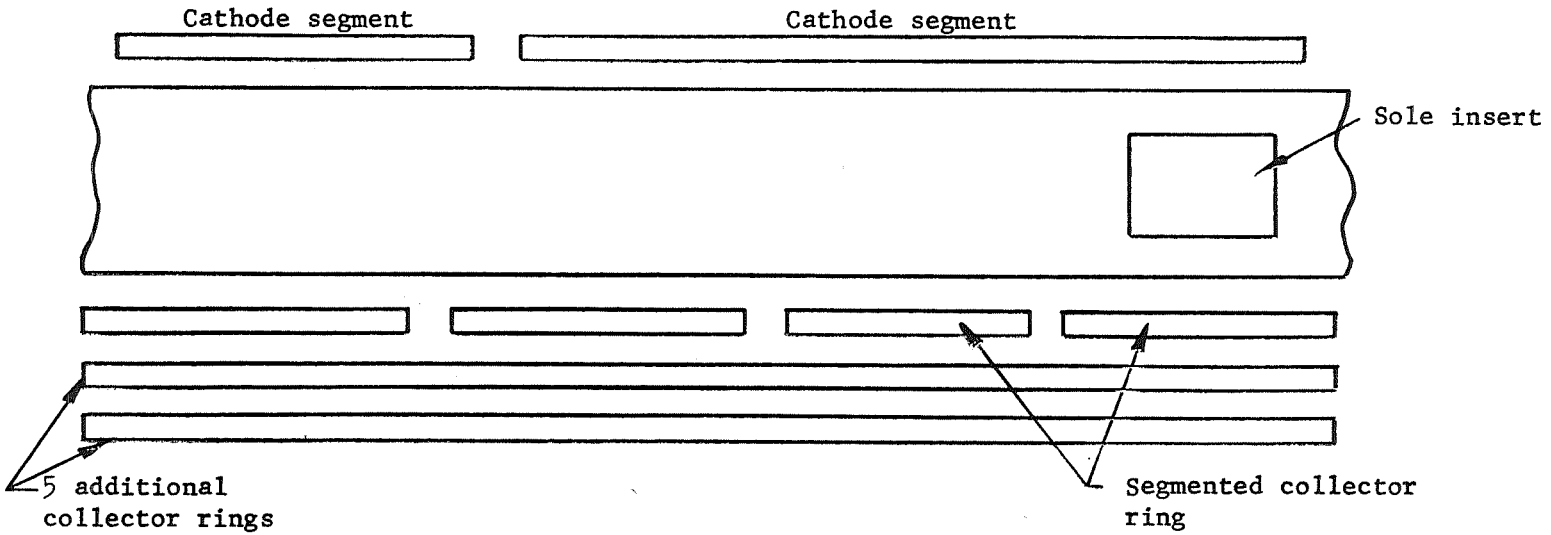

a. Unwrapped interaction space as view from anode

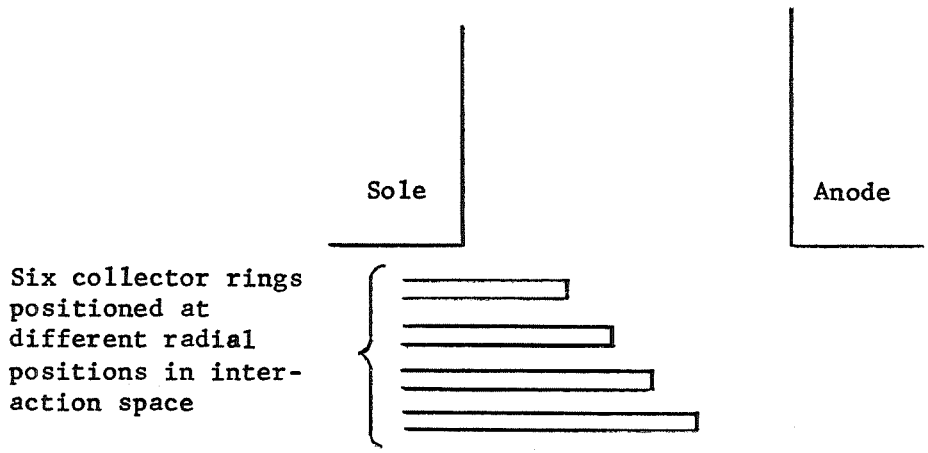

b. End view of interaction space showing positioning of collectors

FIGURE 27 SCHEMATIC DIAGRAM OF ELECTRON OPTICAL SYSTEM FOR UHF AMPLIFIER BUILT ON THIS PROGRAM

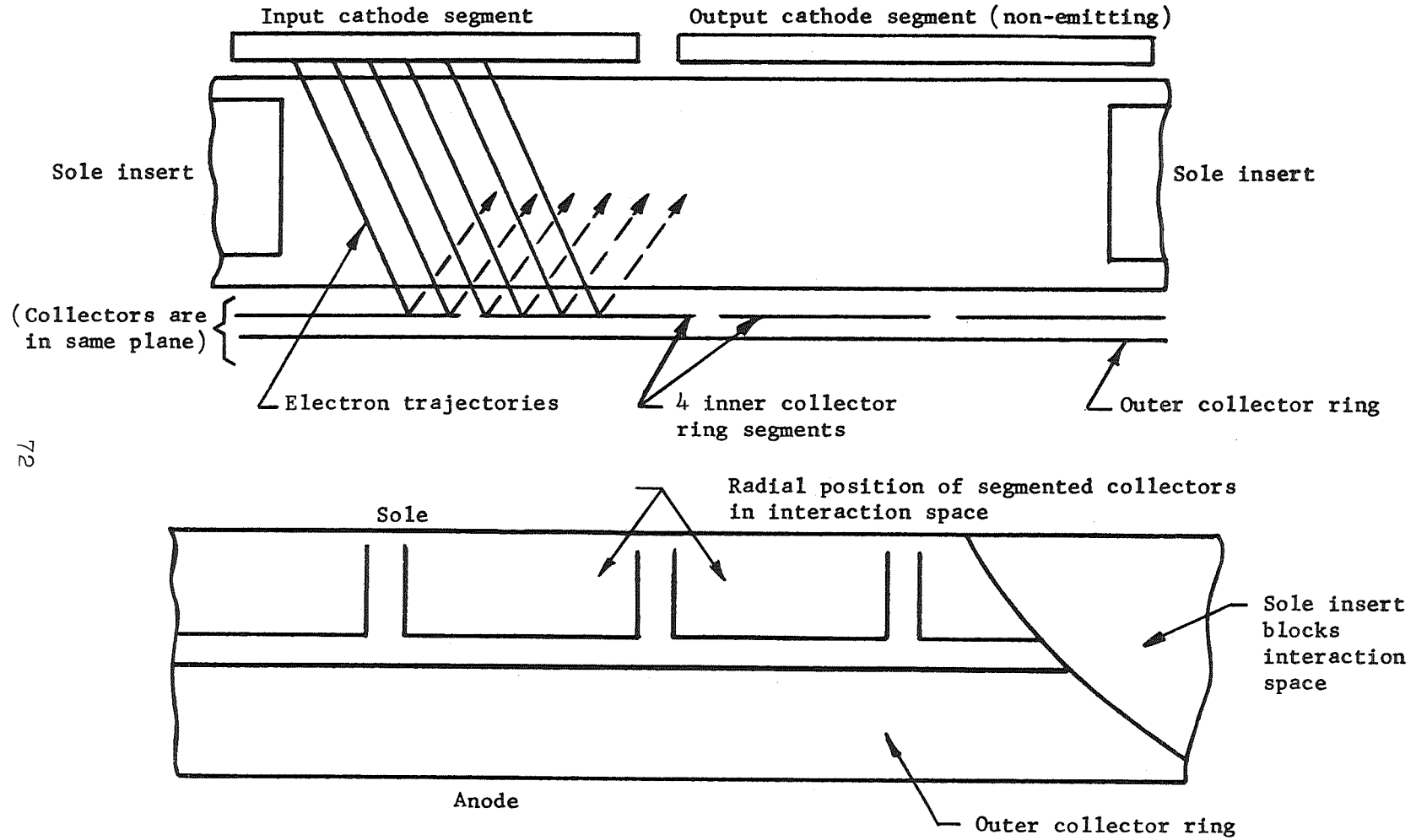

FIGURE 28 AMPLIFIER CONFIGURATION USED ON OTHER PROGRAM

just mentioned. Reentrancy through the drift space was physically blocked by an isolated sole insert. The collector assembly consists of two coplanar collectors which can operate under partial or full beam reflection. The portion of the cathode structure which emits is of limited length and multiple reflections of the relatively high axial velocity electrons are indicated. In tests, this amplifier demonstrated that zero signal stability was attainable even under full beam reflection conditions and proper low noise performance was also obtained with various degrees of beam reflection. The beam used in this amplifier has an appreciable axial velocity component even in the amplifier as built on this program.

When operating with full beam reflection conditions, this amplifier's collector design reduces to essentially a single collector element being operated at ground potential. Although the simple scheme of incorporating a single blocking element in the drift space reduces the obtainable efficiency, the tests performed on this amplifier demonstrated that zero signal stability and high saturation efficiency could be obtained simultaneously from an axial injection system using a reflecting mode of operation.

This amplifier demonstrated 55% efficiency at the 1 kw to 2 kw saturation power output level with zero signal stability.

It is to be emphasized that this efficiency was obtained with what was simply a one- or two-element collection system depending upon how the voltages were adjusted. A more suitable version of the scheme will be sketched in Section 4.0, which gives the conclusions and recommendations for further design development.

4.0 CONCLUSIONS AND RECOMMENDATIONS

4.1 Conclusions From This Program

The ability of an axial injection crossed-field amplifier to provide the optimum operating characteristics for amplification of AM and FM TV signals has been investigated experimentally. The following results and variations from the original design concept have resulted from this work.

The model used to calculate the low level gain of the amplifier is valid and correlates the experimental results.

In emitting sole amplifiers, a drift space transmits electrons from the output to input portions of the reentrant circuit. This demodulates the beam and prevents RF regeneration due to electron reentrancy. This scheme is not adequate to prevent the buildup of background noise for an axial injection amplifier under low RF drive level conditions, and therefore an appropriate design for linear operation should eliminate electron reentrancy.

In axial injection CFAs of the type studied, the electron trajectories cannot be slowed in the axial direction to the degree required to make the electrons circulate around a substantial fraction of the circumference of the tube in one axial transit across the interaction space. As a consequence, many of the electrons leave the interaction space without substantial energy exchange with the RF wave and efficiency is reduced. By reflecting electrons at the sides of the interaction space rather than collecting them, more nearly complete interaction is obtained and the efficiency is high.

The ability to achieve an efficiency of about 70% at the saturation power level using total beam reflection has been demonstrated. Noise levels are low when the tube is operated as a saturated amplifier under this condition, but there is no dynamic range.

Gain of 20 db and wide dynamic range have been demonstrated when electron reentrancy is inhibited.

The axial injection amplifier uses a multi-element collector structure so that the dc power input to the device is a function of the RF drive level, thus maintaining conversion efficiency over a wide range of RF drive levels. An effective demonstration of the collector operation was not achieved. This is believed to be primarily due to the improper positioning of an auxiliary electrode which fills the transition space between the anode circuit and the collector structure. The effects of the field deformation due to this electrode were probably compounded by secondary emission from some of the collector elements. A new collector format appropriate to a non-reentrant design will be suggested. A full test of beam reflection operation could not be achieved on this amplifier. However, the results of large signal computer runs and experimental results achieved from other axial injection amplifier programs support the validity of this concept.

It is therefore proposed that with the proper modification in design approach, the axial injection crossed-field amplifier is well suited for providing high conversion efficiency over a wide range of drive levels.

High gain level, zero signal stability, low cathode emission density, uniform thermal dissipation on the circuit, and long life capability should be resultant operating characteristics.

4.2 Suggested Modifications in Design Approach

There is an accumulation of evidence that the desirable characteristics of the axial injection amplifier can be achieved with the following modifications in the format of the original concept. These involve blocking the electron stream reentrancy in order to avoid undesirable background noise in the absence of RF drive. In addition, a scheme of reflection from the end spaces is needed to

compensate for the relatively high axial velocities in the beam so that an adequate level of circulating current can be maintained at a reasonable level of cathode current. The limited circumferential distance traveled during each axial transit of the electrons reduces the importance of the original concept of reentrancy. A non-reentrant approach makes invalid the use of a full circle cathode, since the current injected near the output region of the tube would be largely wasted, and therefore distributed emission is to be maintained but with a cathode segment that covers only a fraction of the circuit circumference. The concept of a multi-element collector to receive the spent electrons at a potential approximately equal to that with which they exit from the interaction space is retained. This continues to provide the capability for maintaining a high level of efficiency over wide range of drive level.

A method of combining the original axial injection amplifier approach with the modifications ust enunciated is illustrated in Figure 29. It is seen here that a cathode segment of limited circumferential length provides the current. The beam reflection occurs at the end spaces at either axial terminal of the interaction space. A multi-element collector system is now placed in line with the circumferential velocity vector of the electron stream rather than in the end space as was done in the present program. Thus, the collector structure serves a dual purpose. It prevents electron stream reentrancy while at the same time providing a sequence of potential levels appropriate to the degree of RF modulation existing on the spent beam. It is believed that these modifications to the original format of the axial injection amplifier concept will lead to a full realization of its potential capabilities.

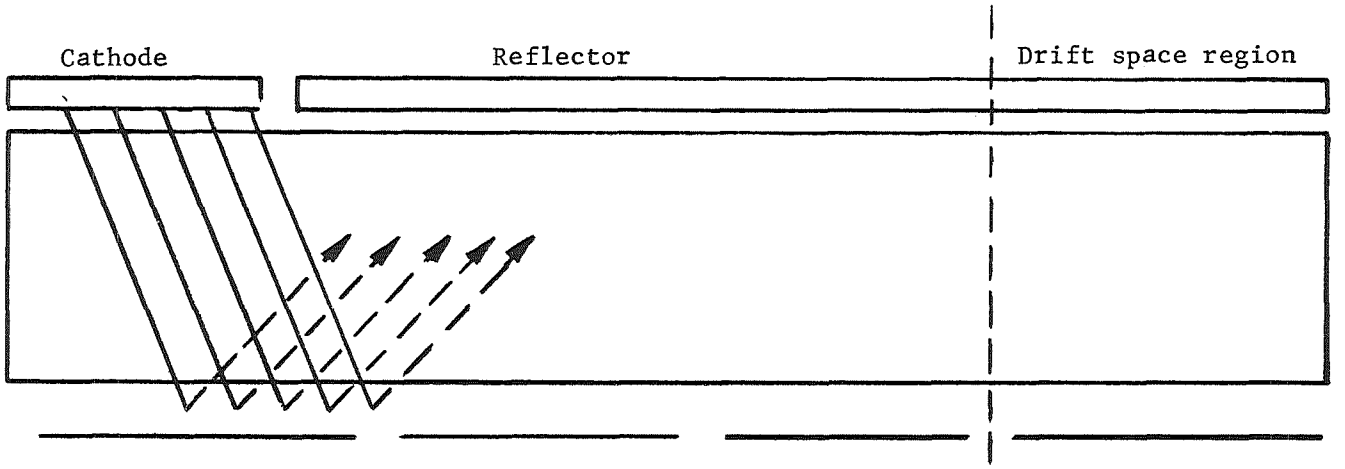

a. Unwrapped interaction space as seen from the anode

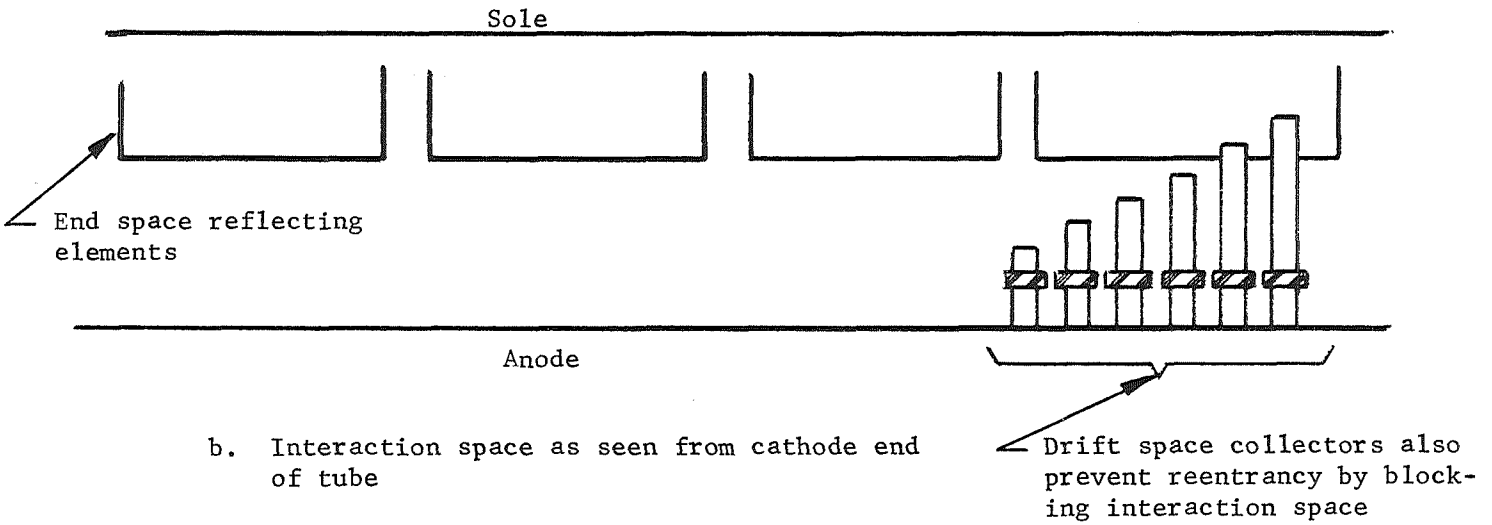

b. Interaction space as seen from cathode end of tube

FIGURE 29 SUGGESTED MODIFICATION OF AMPLIFIER DESIGN

REFERENCES

1. R.G.E. Hutter, BEAM AND WAVE ELECTRONICS IN MICROWAVE TUBES, D. Van Nostrand Co., 1960, pp 260-281

2. G.S. Kino and N.J. Taylor, "The Design and Performance of A Magnetron Injection Gun," IRE Trans Electron Devices, Vol 9, No. 1, January 1962, pp 1-11

3. H.L. McDowell, "A Half Octave Bandwidth X-band Crossed-field Amplifier (U)", S-F-D laboratories/A Varian Division, Final Report, Contract F30602-69-C-0205 (Rome Air Development Center), Secret Report (approximate publication date - May 1970)

(U) DISTRIBUTION LIST

Contract NAS12-653	Copies
Nasa Headquarters, Washington, D.C. 20546	
Attn: A.M. Greg Andrus, Code SAC	1
O. Stanton, Code RET	1
Langley Research Center, Attn: B.M. Kendall, M.S. 473, Langley Station, Hampton, Virginia 23365	1
Lewis Research Center, 21000 Brookpark Road, Cleveland, Ohio 44135	
Attn: P. Ramins, M.S. 54-3	1
H.G. Kosmahl, M.S. 54-3	1
Geo. C. Marshall Space Flight Center, Attn: E.C. Hamilton, Code R-ASTRA-A, Marshall Space Flight Center, Alabama 35812	1
Jet Propulsion Laboratory, Attn: Lloyd Derr, M.S. 161-218, 4800 Oak Grove Drive, Pasadena, California 91103	1
Electronics Research Center, 575 Technology Square, Cambridge, Massachusetts 02139	
Attn: Robert Woolson, Code ANP (Reproducible master)	15
C.M. Veronda, Code ROI	1
Manned Spacecraft Center, Houston, Texas 77058	
Attn: Joe Fowler, EE3	1
M.W. Hamilton, EE3	1
USAECOM, Attn: H. Hersh, Code AMSEL-KL-TM, Fort Monmouth, New Jersey 07703	1
RADC, Attn: H. Chiosa, Code EMATE, Griffiss Air Force Base, New York 13440	1
Naval Research Laboratory, Attn: Dr. S.T. Smith, Code 5240, Washington, D.C. 20390	1
Advisory Group on Electron Devices, Attn: C. Vogel, 8th Floor, 201 Varick Street, New York, New York 10014	1
NESCOM, Attn: T. Marchese, Code 05143A4A, Navy Department, Washington, D.C. 20360	1
University of Florida, Attn: Professor A. Sutherland, Electrical Engineering Department, Gainesville, Florida 32601	1

Contract NAS12-653	Copies
Communication Research Center, Attn: Mr. Roger Aiken, Shirley Bay, Box 490 Terminal A, Ottawa 2, Ontario, Canada	1
University of Florida, Attn: Professor A. Sutherland, Electrical Engineering Department, Gainesville, Florida 32601	1
General Electric Company, Attn: R. Swartley, Space Systems Division, Valley Forge, Pennsylvania 19481	1
General Electric Company, Tube Operations, Schenectady, New York 12305	1
Hughes Aircraft Company, Attn: Technical Librarian, Culver City, California 90230	1
Hughes Aircraft Company, Electron Device Division, Torrance Airport, Torrance, California 90509	1
ITT Tube Division, Easton, Pennsylvania 18042	1
Litton Industries, Electron Tube Division, 960 Industrial Way, San Carlos, California 94070	1
M.I.T., Lincoln Laboratory, Attn: G. Gurnsey, Lexington, Massachusetts 02173	1
University of Michigan, Attn: Professor J.E. Rowe, Electrical Engineering Department, Ann Arbor, Michigan 48104	1
Microwave Associates, Burlington Industrial Park, Burlington, Massachusetts 01803	1
Microwave Electronics Corporation, Division of Teledyne, Palo Alto, California 94304	1
RCA, Defense Communication System Division, Attn: Frank Klawsnik, Moorestown, New Jersey 08057	1
RCA Tube Operations, Lancaster, Pennsylvania 17604	1
Raytheon Tube Division, Willow Street, Waltham, Massachusetts 02154	1
Sanders Associates, Attn: Mr. Frank Hardy, Crosby Road, Bedford, Massachusetts 01730	1

NAS12-653

	Copies
TRW Systems Incorporated, 1 Space Park, Redondo Beach, California 90278	
Attn: J. Jansen	1
Scot McCaskey	1
Watkins-Johnson Company, Attn: O.T. Purl, 3333 Hillview Avenue, Palo Alto, California 94304	1